Cell Reports

Article

The P-body protein 4E-T represses translation to regulate the balance between cell genesis and establishment of the postnatal NSC pool

Graphical abstract

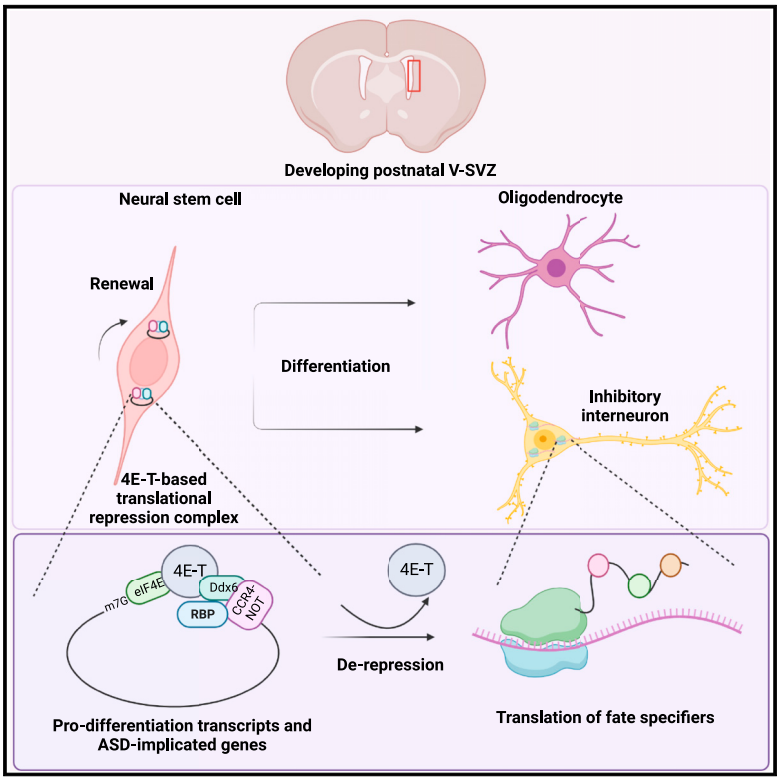

Authors

Adelaida Kolaj, Siraj K. Zahr, Beatrix S. Wang, ..., Guang Yang, David R. Kaplan, Freda D. Miller

Correspondence

freda.miller@msl.ubc.ca

In brief

Kolaj et al. show that in neural stem cells during postnatal times, 4E-T regulates the balance between cell genesis and stem cell expansion by translationally repressing mRNAs encoding transcriptional regulators. 4E-T ensures that neurogenesis occurs at the appropriate times and amounts and that the stem cell pool is not depleted.

Highlights

- Postnatal neural stem cells express neurogenic mRNAs, but not their proteins
- The translational regulator 4E-T sequesters and represses these mRNAs in P-bodies
- 4E-T loss derepresses neurogenic mRNAs, resulting in aberrant neurogenesis
- 4E-T ensures the stem cell pool is not depleted during a time of rapid cell genesis

Kolaj et al., 2023, Cell Reports *42*, 112242
March 28, 2023
https://doi.org/10.1016/j.celrep.2023.112242

CellPress

Cell Reports

CellPress
OPEN ACCESS

Article

The P-body protein 4E-T represses translation to regulate the balance between cell genesis and establishment of the postnatal NSC pool

Adelaida Kolaj,[1,2] Siraj K. Zahr,[1,4] Beatrix S. Wang,[1,4,10] Taylor Krawec,[5] Hilal Kazan,[9] Guang Yang,[5,6,7,8] David R. Kaplan,[1,3,4,11] and Freda D. Miller[1,2,3,4,10,11,12,*]

[1]Program in Neuroscience and Mental Health, Hospital for Sick Children, Toronto, ON M5G1L7, Canada
[2]Department of Physiology, University of Toronto, Toronto, ON M5G 1A8, Canada
[3]Department of Molecular Genetics, University of Toronto, Toronto, ON M5G 1A8, Canada
[4]Institute of Medical Sciences, University of Toronto, Toronto, ON M5G 1A8, Canada
[5]Department of Medical Genetics, Cumming School of Medicine, University of Calgary, Calgary, AB T2N 1N4, Canada
[6]Department of Biochemistry and Cell Biology, Cumming School of Medicine, University of Calgary, Calgary, AB T2N 1N4, Canada
[7]Hotchkiss Brain Institute, Cumming School of Medicine, University of Calgary, Calgary, AB T2N 1N4, Canada
[8]Owerko Centre, Alberta Children's Hospital Research Institute, University of Calgary, Calgary, AB T2N 1N4, Canada
[9]Department of Computer Engineering, Antalya Bilim University, Antalya, Turkey
[10]Michael Smith Laboratories, University of British Columbia, Vancouver, BC V6T 1Z4, Canada
[11]Department of Medical Genetics, University of British Columbia, Vancouver, BC V6T 1Z4, Canada
[12]Lead contact
*Correspondence: freda.miller@msl.ubc.ca
https://doi.org/10.1016/j.celrep.2023.112242

SUMMARY

Here, we ask how developing precursors maintain the balance between cell genesis for tissue growth and establishment of adult stem cell pools, focusing on postnatal forebrain neural precursor cells (NPCs). We show that these NPCs are transcriptionally primed to differentiate and that the primed mRNAs are associated with the translational repressor 4E-T. 4E-T also broadly associates with other NPC mRNAs encoding transcriptional regulators, and these are preferentially depleted from ribosomes, consistent with repression. By contrast, a second translational regulator, Cpeb4, associates with diverse target mRNAs that are largely ribosome associated. The 4E-T-dependent mRNA association is functionally important because 4E-T knockdown or conditional knockout derepresses proneurogenic mRNA translation and perturbs maintenance versus differentiation of early postnatal NPCs in culture and *in vivo*. Thus, early postnatal NPCs are primed to differentiate, and 4E-T regulates the balance between cell genesis and stem cell expansion by sequestering and repressing mRNAs encoding transcriptional regulators.

INTRODUCTION

During postnatal development, tissue-resident stem cells must both support high-level cell genesis for tissue growth and generate adult stem cell pools. How is the balance between cell genesis versus stem cell expansion achieved? One important mechanism during embryogenesis is transcriptional priming, where differentiation-associated mRNAs are transcribed in precursor cells, but their translation is repressed.[1–4] These primed precursors can then be rapidly recruited for differentiation without depleting the precursor pool.[5–7]

Is translational repression also important during postnatal tissue growth? The brain, and in particular the cortex, is one place where this may be the case. This is because, during the first 3 postnatal weeks, there is genesis of most cortical glial cells and of prefrontal cortex and olfactory bulb neurons.[8,9] At the same time, the forebrain ventricular-subventricular zone (V-SVZ) neural stem cell (NSC) pool is generated,[10,11] with developing NSCs undergoing a gradual transition to achieve their final adult dormant state.[12,65,66] Whether translational repression regulates these two events is still an open question, although several studies[14,15] have documented post-transcriptional regulatory mechanisms in adult V-SVZ neural precursor cells (NPCs) and in embryonic cortical precursors (reviewed in Zahr et al.[4] and Rajman and Schratt[13]).

Here, we have asked two questions to explore the possibility of translational repression in postnatal V-SVZ NPCs. First, we have asked whether these precursors are transcriptionally primed, and we provide evidence that this is indeed the case. Second, we have asked how these primed precursors are maintained in an undifferentiated state, focusing on two known translational repressors. One of these is 4E-T, a protein we previously showed silences pro-differentiation mRNAs in embryonic cortical precursors to ensure appropriate neurogenesis.[6,7] 4E-T does this by binding to RNA-binding proteins (RBPs), such as Smaug and Pumilio,[5–7] and sequestering these RBPs

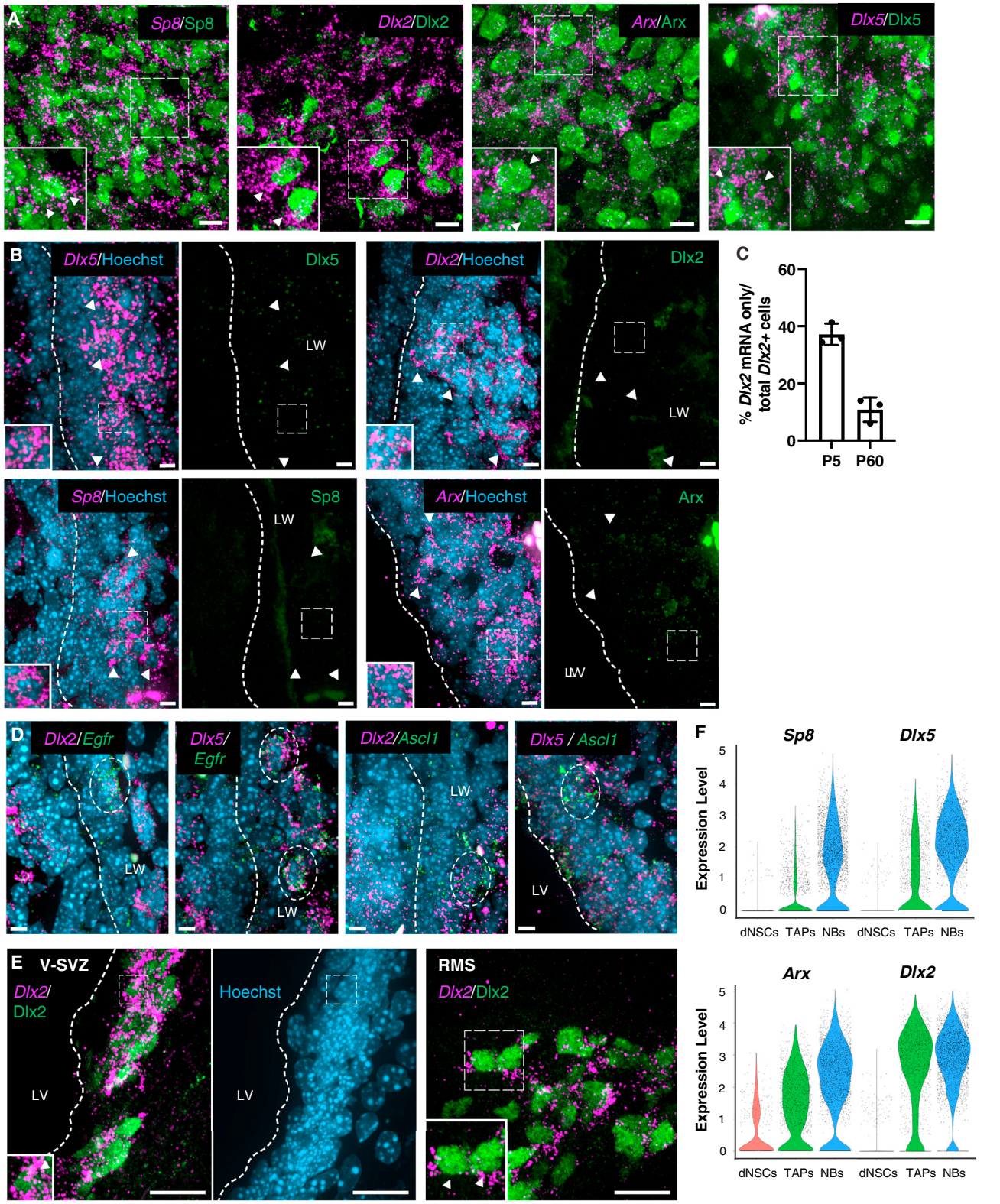

(legend on next page)

and their associated mRNAs in P-bodies, RNA granules that provide a locus for mRNA repression and degradation.[16,17] The second protein we examined is the RBP Cpeb4, which directly binds the 3′ UTR of target mRNAs, recruits poly(A)-tail-modifying complexes, and can either inhibit or promote translation.[18–22] Notably, Cpeb4 deregulation has been implicated in autism spectrum disorder,[23] but we do not yet know whether it promotes or inhibits translation within this context.

In answering these two questions, we provide support for a model where 4E-T sequesters and represses mRNAs encoding transcriptional regulators in primed postnatal NPCs, thus determining the balance between cell genesis and the establishment of adult NSC pools.

RESULTS

Postnatal V-SVZ NPCs are primed for differentiation by expression of proneurogenic mRNAs, but not their encoded proteins

To ask whether V-SVZ NPCs are primed to differentiate, we analyzed four transcription factors involved in olfactory bulb neurogenesis, Dlx2, Dlx5, Sp8, and Arx.[24–33] We analyzed postnatal day 5 (P5) forebrain sections (Figure S1A), combining fluorescence *in situ* hybridization (FISH) and immunostaining to visualize mRNAs and their corresponding proteins. As predicted, neuroblasts within the rostral migratory stream (RMS) expressed both mRNA and protein for all four transcription factors (Figure 1A). By contrast, within the V-SVZ, some cells expressed mRNA, but not the corresponding protein (Figure 1B). Quantification showed that approximately 40% of *Dlx2* mRNA-positive cells in the V-SVZ did not express Dlx2 protein (Figure 1C). At least some of these transcriptionally primed V-SVZ cells were NPCs because they also expressed *Ascl1* and *Egfr*, marker genes expressed in activated NSCs and their transit-amplifying precursor (TAP) progeny (Figure 1D).[34–37] We did not obtain these patterns of hybridization with a control probe (Figure S1B).

We asked whether this phenomenon persisted into adulthood by analyzing the P60 V-SVZ for Dlx2 (see Figure S1A). In contrast with the neonate, approximately 90% of *Dlx2* mRNA-positive adult V-SVZ cells also expressed the protein (Figures 1C and 1E).

We confirmed that many NPCs in the neonatal V-SVZ are transcriptionally primed for olfactory neurogenesis in two ways. First, we analyzed our previously published P6/7 V-SVZ single-cell RNA sequencing (scRNA-seq) dataset;[66] *Dlx2*, *Dlx5*, *Sp8*, and *Arx* mRNAs were all expressed in *Egfr*- and *Ascl1*-positive TAPs and in their neuroblast progeny (Figure 1F). Second, we analyzed embryonic day 15/16 (E15/16) cortical precursor cells cultured for 4.5 days as a model for perinatal NPCs; these precursors generate oligodendrocytes and olfactory bulb interneurons in culture as they do *in vivo* (B.S.W., A.K., and F.D.M., unpublished data). Within these cultures, many cells were positive for *Dlx2*, *Dlx5*, *Sp8*, and *Arx* mRNAs and their corresponding proteins, but some were positive only for the mRNAs (Figure 2A). Many of the latter expressed two NPC protein markers, Nestin and Sox2 (Figure 2B), and some expressed both *Dlx2* and *Egfr* mRNAs, indicating that they were activated NSCs/TAPs (Figure 2C). We did not obtain these patterns of hybridization with a control probe (Figure S1C).

The translational regulators 4E-T and Cpeb4 are localized to intracellular granules in V-SVZ NPCs

These data indicate that some neonatal V-SVZ NPCs are transcriptionally primed. To ask about potential post-transcriptional mechanisms, we focused on 4E-T and Cpeb4. Initially, we confirmed that *4et* and *Cpeb4* mRNAs were expressed in neonatal NSCs and TAPs by analyzing our P6/7 scRNA-seq data (Figure 2D).[66] We then immunostained P5 forebrain sections for the NPC protein Sox2 and 4E-T or Cpeb4. Both proteins were detected in punctate granules in approximately 80%–85% of Sox2-positive V-SVZ NPCs (Figures 2E–2H). A similar analysis at P60 showed that approximately 30% and 80% of adult Sox2-positive V-SVZ cells were also positive for punctate 4E-T or Cpeb4, respectively (Figures 2G and 2H).

We confirmed the neonatal expression patterns by immunostaining perinatal NPC cultures. Both 4E-T and Cpeb4 were localized to punctate foci in Sox2-positive NPCs (Figures 2I and 2J). We also co-labeled cultures for the P-body protein marker Ddx6.[38–40] Almost all 4E-T-positive granules were also positive for Ddx6 (Figure 2K). By contrast, Cpeb4 and Ddx6 granules were largely distinct, although there were some double-positive granules (Figure 2L). Thus, both 4E-T and Cpeb4 are present in NPC granules, with 4E-T predominantly localized to P-body-like structures, consistent with its known P-body association.[38,41,42]

4E-T and Cpeb4 associate with distinct mRNA subsets in postnatal V-SVZ NPCs, with 4E-T selectively enriched for transcriptional regulators

We next asked about 4E-T and Cpeb4 target mRNAs in the neonatal V-SVZ, using a global unbiased approach. We first

Figure 1. Olfactory neuroblast transcription factors are expressed at the mRNA level in postnatal precursors *in vivo*

(A and B) Representative images of FISH (magenta dots) for mRNA and immunostaining (green) for protein for *Sp8*, *Dlx2*, *Arx*, and *Dlx5* in coronal P5 sections of the RMS (A) or V-SVZ (B). In (B), left panels show FISH and Hoechst 33258 (blue), and right panels show immunostaining of the same field. Boxed regions are shown in the insets, and arrowheads denote cells positive for mRNA and protein (A) or mRNA only (B).

(C) Scatterplot of the percentage of total *Dlx2* mRNA-positive cells that express *Dlx2* mRNA, but not Dlx2 protein, in the P5 and P60 V-SVZ, determined from images as in (B) and (E) (n = 3 animals each, ≥5 sections/animal). Error bars, standard deviation (SD).

(D) Representative FISH images of P5 sections as in (B) for *Dlx2* or *Dlx5* mRNAs (magenta dots) and either *Egfr* or *Ascl1* mRNAs (green dots). White circles indicate double-positive cells.

(E) Representative images of FISH and immunostaining for *Dlx2* mRNA (magenta dots) and Dlx2 protein (green) in the P60 lateral V-SVZ (left two images) or RMS (right image). Boxed regions are shown in insets, and arrowheads denote double-positive cells.

(F) Violin plots of P6/7 V-SVZ scRNA-seq data[66] for *Sp8*, *Dlx5*, *Arx*, and *Dlx2* mRNAs in dormant NSCs (dNSC), transit-amplifying precursors (TAPs), and neuroblasts (NBs), all as defined in.[66] Black dots indicate individual cells.

In (B), (D), and (E), sections were counterstained for Hoechst 33258 (blue), and hatched lines denote the boundary between the lateral wall (LW) and lateral ventricle (LV). Scale bars, 5 μm (A, B, and D); 15 μm (E). See also Figure S1.

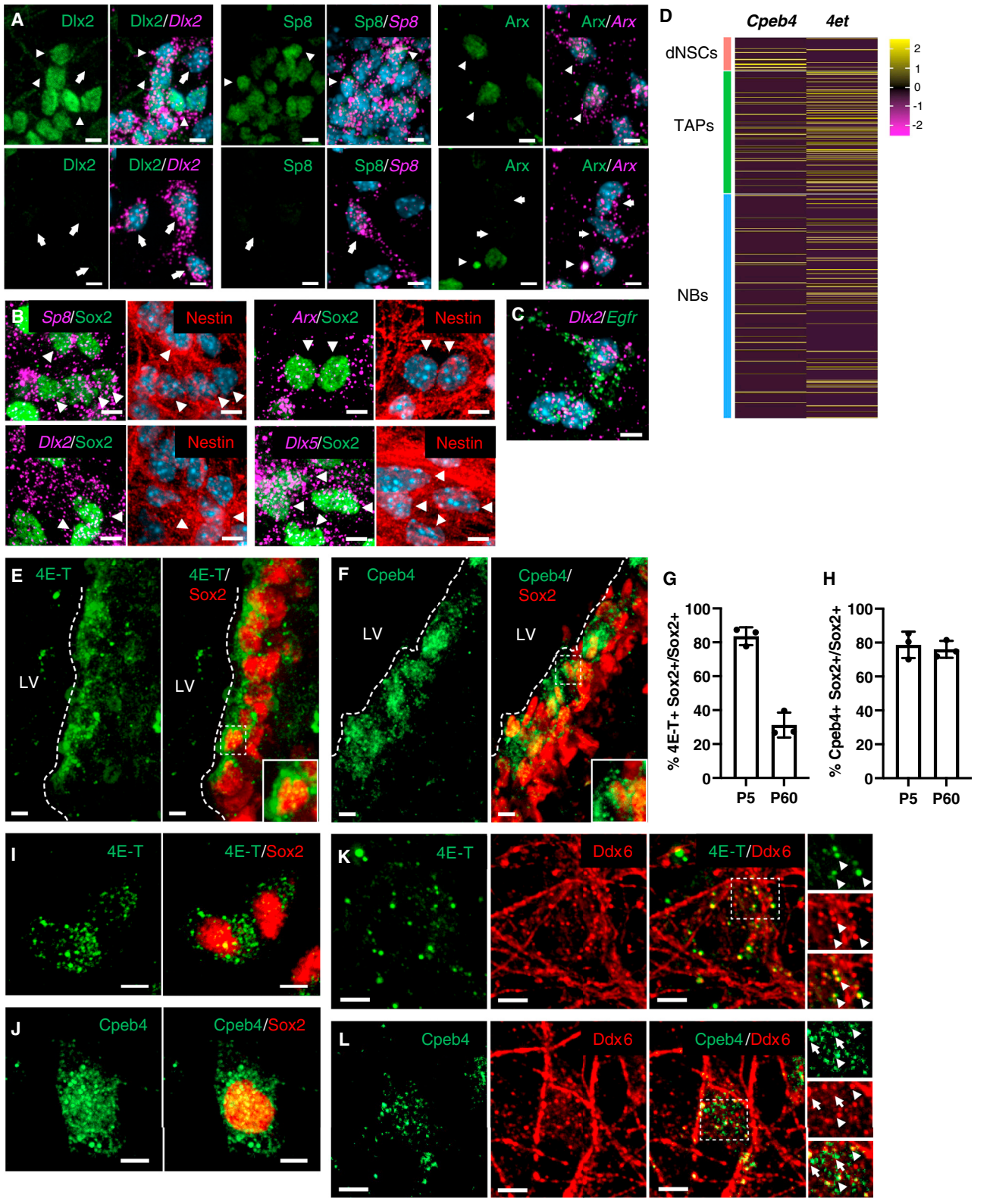

(legend on next page)

immunoprecipitated 4E-T from P7/8 V-SVZ lysates and sequenced the associated mRNAs (RNA immunoprecipitation sequencing [RIP-seq]), performing similar immunoprecipitations with a non-specific IgG as a control. Western blots showed that 4E-T was immunoprecipitated with anti-4E-T, but not with a control IgG (Figure 3A). Sequencing identified 1,259 mRNAs that were at least 2-fold enriched in the 4E-T immunoprecipitates relative to the control IgG (Table S1). Notably, of the four primed transcription factors we had identified, *Dlx5* and *Arx* mRNAs were 2-fold enriched, while *Dlx2* mRNA was 1.9-fold enriched (Table S1). In contrast, *Sp8* mRNA was not significantly enriched (Table S1), suggesting that another post-transcriptional mechanism might be important for this mRNA.

Gene Ontology using PANTHER (Figure 3B; Table S1) showed that almost half of the enriched 4E-T target mRNAs encoded nucleic acid metabolism proteins, gene-specific transcriptional regulators, and chromatin/chromatin-binding proteins. A similar analysis of molecular function using g:Profiler (Figure 3C; Table S1) showed that among the most significantly enriched categories were mRNAs encoding nucleic acid-binding proteins (477) and transcriptional regulatory proteins (199). Notably, this included transcription factors associated with interneuron differentiation, such as *Dlx5*, *Arx*, *Gsx2*, *Npas4*, *Foxg1*, *Rest*, and *Cux1*,[43–47] and with glial development, such as *Sox6*, *Sox9*, *Sox10*, and *Olig2*.[48–50] The g:Profiler analysis also indicated significant enrichment of mRNAs implicated in CNS aplasia, microcephaly, and morphological development (Figure 3D; Table S1). Consistent with this, 4E-T target mRNAs included 51 class 1 and 2 SFARI autism spectrum disorder (ASD) genes (from https://gene.sfari.org), including many known to regulate NPCs and their differentiation, such as *Ankrd11*, *Arx*, *Atrx*, *Chd7*, *Crebbp*, *Foxg1*, *Kmt2a*, *Ldb1*, *Phf12*, *Phf3*, *Setbp1*, *Smarca2*, *Tcf7l2*, *Upf3b*, and *Zmynd8* (asterisks in Table S1). Analysis of the scRNA-seq data showed that all of these mRNAs were detectably expressed in P6/7 NSCs and TAPs (Figure S2A).

We validated these findings by immunoprecipitating V-SVZ lysates with 4E-T antibody or control IgG and performing qPCR. As predicted, 4E-T immunoprecipitates were enriched for the pro-differentiation and neurodevelopmental disorder mRNAs *Dlx5*, *Dlx2*, *Gsx2*, *Sox9*, *Sox10*, *Olig2*, *Crebbp*, *Foxg1*, *Arx*, and *Chd7* (Figure 3E). Conversely, three non-enriched genes in the 4E-T RIP-seq data, *Rpl18a*, *Rpl8*, and *Ywhaz*, were also not enriched by qPCR (Figure 3E).

We next performed RIP-seq for Cpeb4, immunoprecipitating it from P7/8 V-SVZ lysates. Western blots confirmed Cpeb4 was specifically immunoprecipitated with anti-Cpeb4 and not the control IgG (Figure 3F). Sequencing identified 1,756 protein-coding mRNAs enriched at least 2-fold in Cpeb4 versus control IgG immunoprecipitates (Table S2). Of the 1,755 Cpeb4 target mRNAs, only 4% (78 mRNAs) were shared with 4E-T (Tables S1 and S2). The shared targets did not include *Dlx2*, *Dlx5*, or *Arx* mRNAs.

Gene Ontology using PANTHER showed that Cpeb4 targets were functionally more diverse than 4E-T targets, with the two most enriched categories being protein-modifying enzymes and metabolite interconversion enzymes (Figure 3G; Table S2). g:Profiler analysis confirmed that the most enriched categories in the biological process category were protein modification, biosynthesis, and cellular metabolic processes (Figure 3H; Table S2). The Cpeb4 target mRNAs were also highly enriched for genes associated with neurodevelopmental delay, language impairment, and intellectual disability (Figure 3I), as predicted,[23] and included 64 class 1 and 2 SFARI ASD genes, including *Fmr1*, *Foxp1*, *Tcf7l2*, *Pcdh19*, *Pten*, and *Zmynd11* (Table S2) (from https://gene.sfari.org).

We validated a subset of these Cpeb4 target mRNAs (*Tcf7l2*, *Zmynd11*, *Kcnd2*, *Ldb2*, *Pcdh18*, *Thap1*, *Tshz1*, *Tra2a*, *Zfp322a*, *Sox9*, and *Mex3b*) by qPCR of Cpeb4 immunoprecipitations of P6/7 V-SVZ lysates (Figure 3J). The mRNAs were all enriched relative to the control IgG, but there was no enrichment for *Rpl18a* and *Tubb2*, two non-enriched mRNAs from the RIP-seq analysis (Figure 3J).

Identification of 4E-T and Cpeb4 target mRNAs in cultured V-SVZ NPCs

These data indicate that 4E-T and Cpeb4 associate with distinct mRNA populations in the postnatal V-SVZ. To determine whether either protein functioned as a repressor, we identified ribosome-associated mRNAs in P7 V-SVZ NPCs cultured as neurospheres for 1 week. As a prelude to this analysis, we characterized 4E-T and Cpeb4 mRNA targets in these cultured neurospheres. We initially immunoprecipitated 4E-T, confirming the specificity of the pull-down relative to a control IgG (Figure 4A). Sequencing identified 1,089 associated protein-coding mRNAs

Figure 2. Characterization of the expression of 4E-T, Cpeb4, and proneurogenic transcription factors in postnatal precursors in culture and *in vivo*

(A and B) Representative images of cultures of E15/16 cortical cells analyzed after 4.5 days by FISH for *Dlx2*, *Sp8*, and *Arx* mRNAs (magenta dots) and immunostaining for the corresponding proteins (A, green) or for Sox2 (B, green) and Nestin (B, red). Cells were also counterstained with Hoechst 33258 (blue). In (A), arrowheads denote cells positive for both mRNA and protein, and arrows for mRNA only. In (B), arrowheads denote triple-labeled cells.

(C) Representative FISH image of cells cultured as in (A) and (B), analyzed for *Dlx2* (magenta) and *Egfr* (green) mRNAs, and counterstained with Hoechst 33258 (blue).

(D) Single-cell heatmap of P6/7 V-SVZ scRNA-seq data[66] showing *4et* and *Cpeb4* mRNAs in dNSCs, TAPs, and neuroblasts (as defined in Borrett et al.[66]). Expression levels are coded as per the adjacent key.

(E and F) Representative images of coronal P5 V-SVZ sections immunostained for Sox2 (red) and 4E-T (E, green) or Cpeb4 (F, green). Double-positive cells in boxed regions are shown in insets. Hatched lines denote the LV boundary.

(G and H) Scatterplots showing the percentage of total Sox2-positive V-SVZ cells detectably expressing punctate 4E-T (G) or Cpeb4 (H) at P5 and P60 (n = 3 animals each; $\geq$5 sections/animal). Error bars = SD.

(I and J) Representative images of cells cultured as in (A) and (B) immunostained for Sox2 (red) and 4E-T (I, green) or Cpeb4 (J, green).

(K and L) Representative images of cells cultured as in (A) and (B) and immunostained for Ddx6 (red) and 4E-T (K, green) or Cpeb4 (L, green). Boxed areas are shown to the right, and arrowheads indicate granules positive for Ddx6 and 4E-T or Cpeb4. In (L), arrows indicate Cpeb4-positive, Ddx6-negative granules. Scale bars, 5 μm.

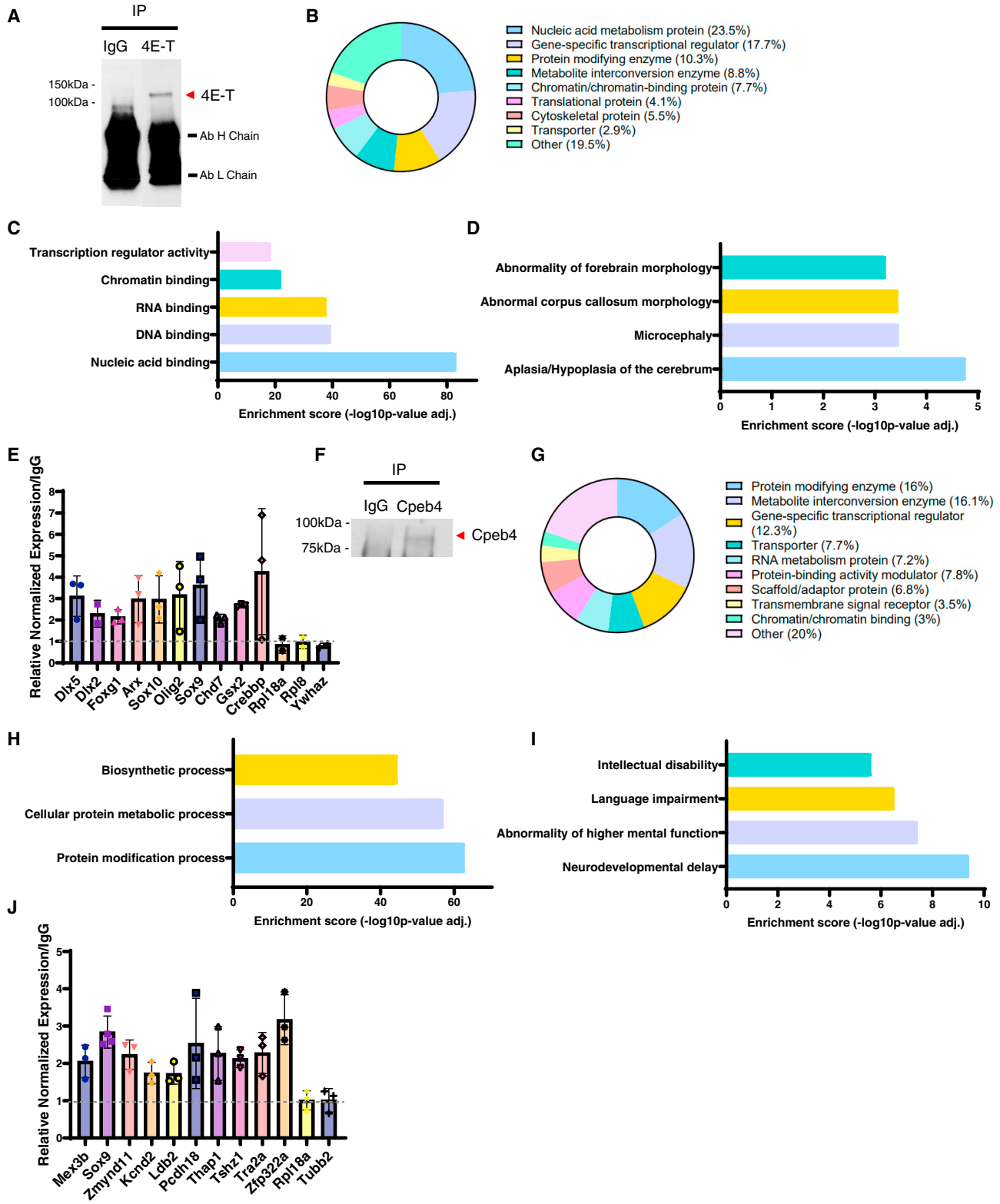

Figure 3. 4E-T and Cpeb4 associate with distinct mRNA subsets in the postnatal V-SVZ

(A) Western blot of anti-4E-T or nonspecific IgG immunoprecipitates from the P7/8 V-SVZ, probed for 4E-T (red arrowhead). Molecular weight markers are shown on the left, and Ab H chain and Ab L chain are IgG heavy and light chains, respectively.

(legend continued on next page)

that were enriched at least 1.75-fold in 4E-T versus control IgG immunoprecipitates (Table S3). Gene Ontology identified nucleic acid-binding proteins as highly enriched; of 1,089 total mRNAs, 378 encoded nucleic acid-binding proteins (Table S4). The dataset was also highly enriched for transcription and gene expression mRNAs, as well as for cell-cycle and metabolic process genes (Figure 4B; Table S4), the latter two potentially because NPCs in neurospheres are highly proliferative. A total of 237 of the 4E-T neurosphere targets were shared with the V-SVZ target dataset (Table S3), likely representing NPC-enriched target mRNAs. More than half (121) of these were nucleic acid-binding protein mRNAs (Table S5). The shared targets also included SFARI ASD genes (from https://gene.sfari.org), such as *Ankrd11*, *Arx*, *Baz2b*, *Brd4*, *Chd7*, *Crebbp*, *Jmjd1c*, *Ncor1*, *Setd2*, *Sox6*, *Tcf7l2*, and *Zmynd8*, but did not include *Dlx5*, *Dlx2*, *Gsx2*, or *Foxg1*, likely because neurosphere cultures bias NPCs to differentiate into glia rather than interneurons.

We performed qPCR of 4E-T neurosphere immunoprecipitates to validate this dataset. The 4E-T target mRNAs *Chd7*, *Sox6*, *Tcf7l2*, *Arid1b*, *Baz2b*, *Top2a*, *Kmt2a*, *Nrcam*, *Setd2*, *Plxnb2*, *Pola2*, *Srsf3*, and *Mcm4* were all enriched, whereas two mRNAs that were non-enriched in the 4E-T RIP-seq, *Rpl4* and *Rpl7*, were also not enriched in the qPCRs (Figure 4C).

We performed a similar RIP-seq analysis for Cpeb4, initially confirming specific immunoprecipitation of Cpeb4 from neurospheres (Figure 4D). Sequencing identified 1,106 protein-coding mRNAs that were enriched at least 1.75-fold in Cpeb4 versus control IgG immunoprecipitates (Table S6). Of these, only 61 were shared with 4E-T (Table S6). Gene Ontology (Figure 4E; Table S6) showed that these targets were most enriched for categories such as cellular metabolism, macromolecular modification, and cellular localization. About half (536) of the neurosphere targets were also Cpeb4 targets in the V-SVZ (shown in Table S6). We validated this dataset by performing qPCR on Cpeb4 versus IgG neurosphere immunoprecipitates. As predicted from the RIP-seq, the Cpeb4 target mRNAs *Pten*, *Cdh10*, *Cdh11*, *Mcm4*, *Pola2*, *Ythdf2*, and *Srsf3* were all enriched, whereas *Rpl9* mRNA was not (Figure 4F).

4E-T, but not Cpeb4, target mRNAs are selectively depleted from NPC ribosomes

We next asked whether 4E-T and/or Cpeb4 target mRNAs were ribosome associated in NPCs cultured as neurospheres. To do this, we used mice carrying a floxed allele of an hemagglutinin (HA)-tagged ribosomal protein, RPL22,[80] and a well-characterized *Nestin-CreERT2* allele.[51] We grew P7/8 V-SVZ neurospheres from these mice for 5 days and treated them with tamoxifen for 2 additional days, which should result in expression of HA-tagged ribosomes in Nestin-positive NPCs (Figure 5A).[52–54] We confirmed that, as predicted, HA-tagged RPL22 was detectable in tamoxifen-treated *Nestin-CreERT2;Rpl22*$^{HA/HA}$, but not *Rpl22*$^{HA/HA}$, neurospheres (Figure 5B), and then we immunoprecipitated lysates with anti-HA or a control IgG (Figure 5C).

We sequenced the co-precipitated RNAs, determined fold enrichment in anti-HA versus control IgG immunoprecipitates, and defined a mRNA as ribosome associated if it was enriched >2.0-fold and ribosome depleted if it was <1.0-fold (Table S7). There was no enrichment in either category when considering total detectable protein-coding mRNAs associated with HA-tagged ribosomes; approximately 26% of the mRNAs were ribosome associated and about 26% were ribosome depleted (Figure 5D; Table S7). By contrast, the distribution of 4E-T neurosphere target mRNAs was significantly skewed; approximately 17% of these were ribosome associated and 36% were ribosome depleted (Figure 5E; Table S7). This differential distribution was not correlated with mRNA abundance as shown by analysis of P8 neurosphere microarray data (Figure 5F; Table S8); the relative expression level distribution was similar for ribosome-associated and ribosome-depleted 4E-T target mRNAs. The situation was different for Cpeb4 neurosphere target mRNAs; approximately 40% of these were ribosome associated and 12% were ribosome depleted (Figure 5G; Table S7). Thus, 4E-T, but not Cpeb4, target mRNAs are preferentially depleted from ribosomes.

We performed three additional analyses to confirm this RiboTag analysis of 4E-T targets. First, Gene Ontology showed that nucleic acid-binding proteins and transcriptional regulators were enriched in ribosome-depleted, but not ribosome-associated, 4E-T targets (Figures 5H and 5I; Table S9). Second, qPCRs of anti-HA immunoprecipitates confirmed that, as predicted by the RIP-seq analysis, *Aldoc*, *Apoe*, *Gfap*, and *Hmmr* mRNAs were all ribosome associated, whereas the 4E-T target mRNAs *Baz2b*, *Ankrd11*, *Arid1b*, *Crebbp*, *Setd2*, *Kmt2a*, *Ncor1*, *Nrcam*, *Sox6*, *Rest*, and *Chd7* were all ribosome depleted (Figure 5J). Third, we performed polysome fractionation and profiling. We cultured neurospheres from the P8 V-SVZ of CD1 mice for

(B) PANTHER protein class Gene Ontology of P7/8 V-SVZ 4E-T target mRNAs (Table S1).
(C and D) g:Profiler Gene Ontology of the P7/8 V-SVZ 4E-T target mRNAs (Table S1), showing selected Biological Process (C) and Human Phenotypes (D) categories (Table S1).
(E) qPCR of anti-4E-T P7/8 V-SVZ immunoprecipitates for select 4E-T target mRNAs from the RIP-seq analysis. *Rpl18a*, *Rpl8*, and *Ywhaz* are not 4E-T targets and were analyzed as controls. Results were normalized to control qPCRs so that 1-fold (line) indicates no difference between anti-4E-T versus nonspecific IgG immunoprecipitates.
(F) Western blot of anti-Cpeb4 or nonspecific IgG immunoprecipitates from the P7/8 V-SVZ, probed for Cpeb4 (red arrowhead). Molecular weight markers are shown on the left.
(G) PANTHER protein class Gene Ontology for P7/8 V-SVZ Cpeb4 target mRNAs (Table S2).
(H and I) g:Profiler Gene Ontology of P7/8 V-SVZ Cpeb4 target mRNAs (Table S2) showing selected Biological Process (H) and Human Phenotype (I) categories (Table S2).
(J) qPCR of anti-Cpeb4 P7/8 V-SVZ immunoprecipitates for select Cpeb4 target mRNAs from the RIP-seq analysis. *Rpl18a* and *Tubb2* are not Cpeb4 targets and were analyzed as controls. Results were normalized to control qPCRs so that 1-fold (line) indicates no difference between anti-Cpeb4 versus nonspecific IgG immunoprecipitates.
See also Figure S2 and Tables S1 and S2.

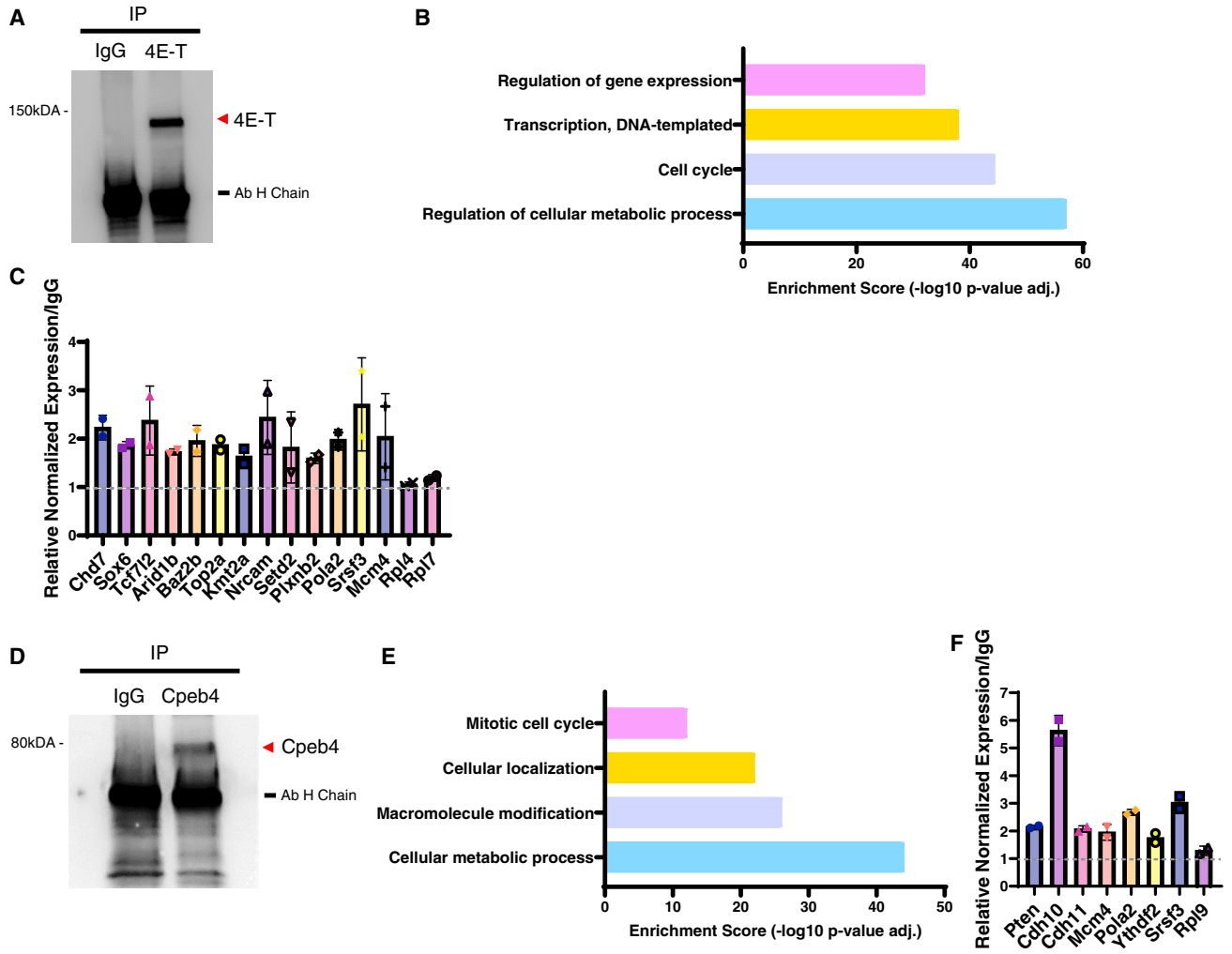

Figure 4. Identification of 4E-T and Cpeb4 target mRNA in P7/8 V-SVZ NPCs cultured as neurospheres

(A) Western blot of anti-4E-T or nonspecific IgG immunoprecipitates from cultured P7/8 primary neurospheres, probed for 4E-T (red arrowhead). Molecular weight marker is shown on the left, and IgG heavy chain is indicated.

(B) g:Profiler Gene Ontology of 4E-T neurosphere target mRNAs showing selected Biological Process categories (Tables S3 and S4).

(C) qPCR of anti-4E-T neurosphere immunoprecipitates for select 4E-T target mRNAs from the RIP-seq analysis. *Rpl4* and *Rpl7* are not 4E-T targets and act as controls. Results were normalized to control qPCRs so that 1-fold (line) indicates no difference between anti-4E-T versus nonspecific IgG immunoprecipitates.

(D) Western blot of anti-Cpeb4 or nonspecific IgG immunoprecipitates from cultured P7/8 primary neurospheres, probed for Cpeb4 (red arrowhead). Molecular weight marker is shown on the left, and the IgG heavy chain is indicated.

(E) g:Profiler Gene Ontology of Cpeb4 neurosphere target mRNAs showing selected Biological Process categories (Table S6).

(F) qPCR of anti-Cpeb4 neurosphere immunoprecipitates for select Cpeb4 target mRNAs from the RIP-seq analysis. *Rpl9* is not a Cpeb4 target and acts as a control. Results were normalized to control qPCRs so that 1-fold (line) indicates no difference between anti-Cpeb4 versus nonspecific IgG immunoprecipitates.

See also Tables S3, S4, S5, and S6.

7 days, treated them with cycloheximide for 10 min, and fractionated polysomes versus monosomes.[55] We performed qPCR on the isolated RNA, normalizing raw values to a spiked *Luciferase* control mRNA. *Aldoc* mRNA, which was ribosome associated and not a 4E-T target (Table S7), was 8- to 15-fold enriched in the polysome versus monosome fraction, confirming the efficacy of the fractionations. Analysis of the 4E-T target mRNAs *Ankrd11*, *Arid1b*, *Baz2b*, *Chd7*, *Kmt2a*, *Ncor1*, *Setd2*, and *Sox6* showed that, relative to *Aldoc* mRNA, all of them were relatively depleted from polysomes (Figure 5K). By contrast, *Apoe*, a second ribosome-associated mRNA that was not a 4E-T target, was enriched in the polysome fraction (Figure 5K).

In cultured perinatal precursors, 4E-T is a translational repressor that regulates the balance between cell genesis and NPC numbers

Based on these findings, we focused our functional studies on 4E-T. Initially, we examined the cultured perinatal cortical precursors, knocking down 4E-T using a previously validated 4E-T shRNA cloned into a piggyBac (PB) expression vector that also

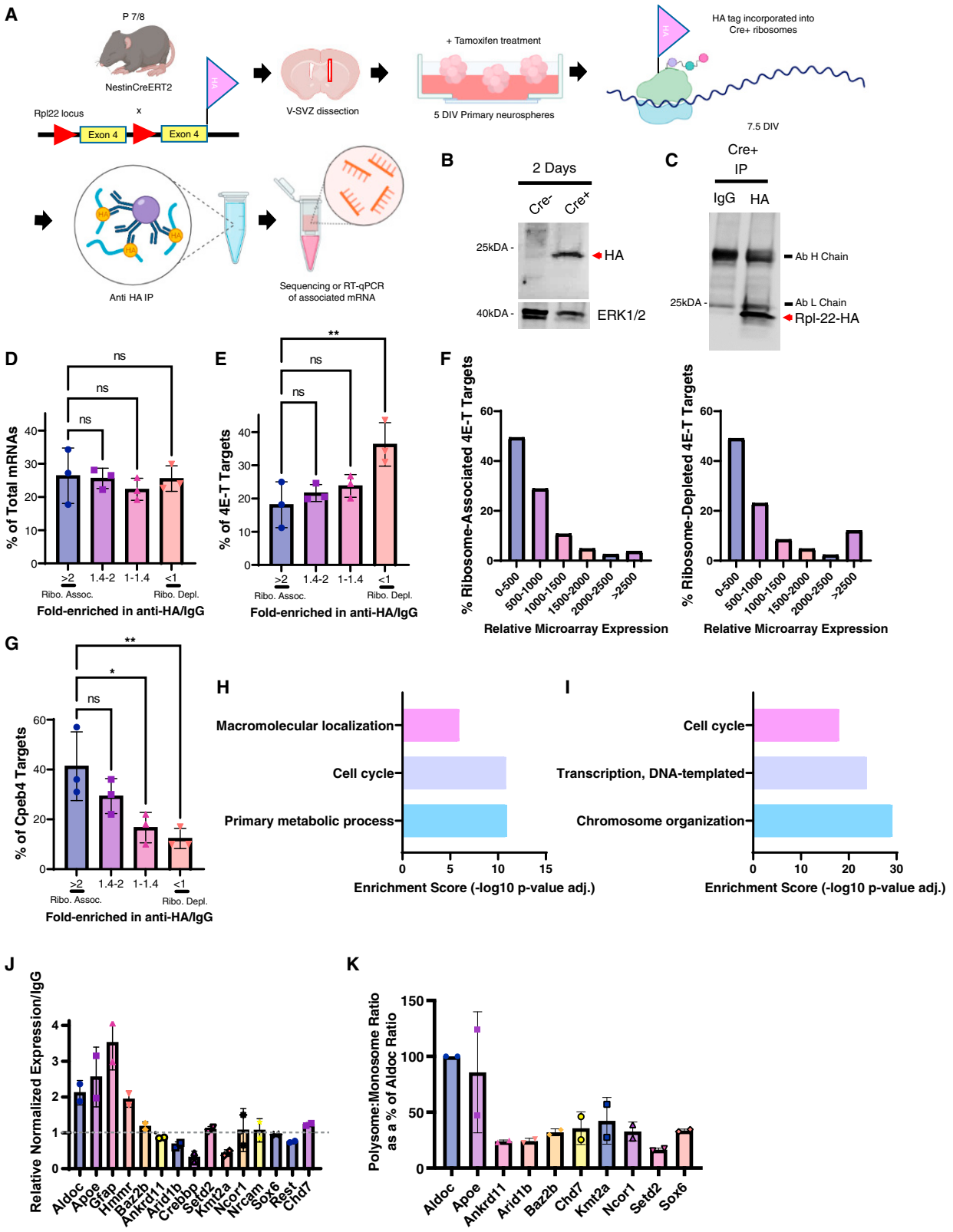

(legend on next page)

encodes turbo GFP (tGFP) and integrates genomically when PB transposase is present.[7] We first confirmed that this shRNA knocked down 4E-T in these perinatal NPCs as it did in earlier cortical precursor cultures (Figure S2B). We then asked whether *4et* knockdown caused derepression and translation of the 4E-T target mRNAs *Dlx2*, *Dlx5*, and *Arx* (Figures 6A–6F). In cultures transfected 4.5 days earlier with a control shRNA, about 8%–18% of tGFP-positive cells detectably expressed Dlx2, Dlx5, or Arx proteins. However, in *4et* shRNA-transfected cultures, tGFP-positive, protein-positive cells were significantly increased 1.5- to 3-fold, indicating that 4E-T normally represses translation of these three proneurogenic mRNAs.

We asked whether this derepression had functional consequences by transfecting cultures with PB transposase and control or *4et* shRNAs and asking about NPCs and cell genesis by immunostaining them 4.5 days later. 4E-T knockdown caused an almost 2-fold reduction in Sox2-positive NPCs and in Sox2-positive, Ki67-positive proliferative NPCs relative to the control shRNA (Figures 6G and 6H). At the same time, βIII-tubulin-positive and NeuN-positive neurons were robustly increased (Figures 6I–6L). By contrast, 4E-T knockdown caused a significant decrease in Olig2-positive, PDGFRα-positive oligodendrocyte progenitor cells (OPCs) (Figures 6M and 6N). Thus, 4E-T knockdown derepressed proneurogenic mRNAs and in so doing depleted NPCs and enhanced neurogenesis at the expense of oligodendrogenesis.

4E-T is essential for maintenance and proliferation of postnatal V-SVZ NPCs *in vivo*

To ask whether 4E-T was similarly important for V-SVZ NPC biology *in vivo*, we generated a mouse carrying a floxed allele of the *4et* gene using mutant C57BL/6 embryonic stem cells (ESCs) obtained from the Knockout Mouse Consortium. These ESCs carried a *4et* allele containing a lacZ trapping cassette in exon 4 (knockout-first allele) (Figure S3A).[56,57] The mutant ESCs were used to generate chimeric mice where the modified *4et* allele was integrated into the germ line. Progeny that were heterozygous for the knockout-first *4et* allele were subsequently crossed to mice expressing flippase (Flp) recombinase (Figures S3A and S3B).[58] Flp-mediated recombination converted the knockout-first allele into a conditional allele containing *loxP* sites flanking critical exon 4 of *4et* (*4et*^{fl}) (Figures S3A and S3C). The *4et*$^{fl/+}$ mice were then backcrossed to wild-type mice for several generations to remove the *Flp* allele and were finally crossed to one another to generate *4et*$^{fl/fl}$ mice. We assessed the successful generation of these mutant alleles using PCR-based strategies (Figure S3).

To validate this mouse for NPC analysis, we crossed it to *Nestin-CreERT2* mice and generated P7/8 V-SVZ neurospheres from progeny that were *4et*$^{fl/fl}$ and that did or did not carry the *Nestin-CreERT2* allele. We treated the neurospheres with tamoxifen for 2 days and performed PCR using primers that distinguish mRNAs transcribed from the floxed versus recombined *4et* alleles. In control *4et*$^{fl/fl}$ neurospheres, there was a single band corresponding to the non-excised allele (Figure 6O). In *Nestin-CreERT2;4et*$^{fl/fl}$ neurospheres, there were two bands corresponding to the non-excised and recombined alleles (Figure 6O), indicating that recombination had occurred but was not complete. We also performed western blots of these neurospheres, using an antibody recognizing the 4E-T amino terminus downstream of the predicted deletion. 4E-T protein was decreased in *Nestin-CreERT2;4et*$^{fl/fl}$ neurospheres relative to *4et*$^{fl/fl}$ neurospheres, and this decrease was tamoxifen dependent (Figures 6P and 6Q).

We used *Nestin-CreERT2;4et*$^{fl/fl}$ mice to ask whether 4E-T was required for neonatal V-SVZ NPCs *in vivo*. We generated litters of *4et*$^{fl/fl}$ neonatal mice with half carrying the *Nestin-CreERT2* allele, exposed them to tamoxifen via their mother's milk from P1 to P3, and injected them with 5-bromo-2′-deoxyuridine (BrdU) at P7. Immunostaining at P8 identified a 48% decrease in V-SVZ BrdU-positive cells in *Nestin-CreERT2;4et*$^{fl/fl}$ versus *4et*$^{fl/fl}$ mice

Figure 5. 4E-T target mRNAs are significantly depleted from cultured NPC ribosomes, whereas Cpeb4 target mRNAs are predominantly ribosome associated

(A) Schematic of the ribosome association experiments.

(B) Western blot of P7/8 *Nestin-CreERT2;Rpl22*$^{HA/HA}$ (Cre^{+}) or *Rpl22*$^{HA/HA}$ (Cre^{-}) neurospheres exposed to tamoxifen for the final 2 of 7 culture days, probed with anti-HA (top, red arrowhead) and reprobed with anti-ERK1/2 (bottom) as a loading control. Molecular weight markers are on the left.

(C) Western blot of anti-HA or nonspecific IgG immunoprecipitates of tamoxifen-treated *Nestin-CreERT2;Rpl22*$^{HA/HA}$ neurospheres, probed for HA-tagged Rpl22 (red arrowhead). Molecular weight marker is to the left, and IgG heavy and light chains are indicated.

(D and E) Protein coding mRNAs identified in three independent experiments as in (A) were analyzed for fold enrichment in anti-HA versus nonspecific IgG immunoprecipitates (Table S7) and were binned based on these fold-changes into four categories: >2-fold (ribosome associated), 1.4- to 2-fold, 1- to 1.4-fold, and <1-fold (ribosome depleted). y axis shows percentage of total mRNAs (D) or 4E-T neurosphere target mRNAs (E; Table S3) in each bin. Each point represents one of three replicate experiments. **$p < 0.01$, one-way ANOVA with Dunnett's multiple comparisons post hoc test.

(F) Percentage of 4E-T neurosphere ribosome-associated (left) and ribosome-depleted (right) target mRNAs with differing relative levels of expression (x axis) in P8 neurosphere microarray data (Table S8).

(G) Cpeb4 neurosphere target mRNAs (Table S6) were analyzed in three independent experiments as in (D) and (E) for fold enrichment in anti-HA versus nonspecific IgG immunoprecipitates. y axis shows percentage of target mRNAs in each bin (Table S7). Each point represents one of three replicate experiments. *$p < 0.05$, **$p < 0.01$, one-way ANOVA with Dunnett's multiple comparisons post hoc test.

(H and I) g:Profiler Gene Ontology for ribosome-associated (H) and ribosome-depleted (I) 4E-T target mRNAs showing selected Biological Process categories (Tables S7 and S9).

(J) qPCR of selected ribosome-associated or ribosome-depleted mRNAs (Table S7) in anti-HA immunoprecipitates of *Nestin-CreERT2;Rpl22*$^{HA/HA}$ neurospheres. Results were normalized to control qPCRs so that 1-fold (line) indicates no difference between anti-HA versus nonspecific IgG immunoprecipitates.

(K) Polysome and monosome fractions from P8 primary wild-type neurospheres were analyzed by qRT-PCR for two ribosome-associated mRNAs that were not 4E-T neurosphere target mRNAs (*Aldoc* and *Apoe*) or for eight ribosome-depleted 4E-T target mRNAs (all others). Raw values were normalized to a spiked *luciferase* control mRNA, and relative enrichments in the polysome versus monosome fractions were expressed as a percentage of the enrichment value for *Aldoc* mRNA (n = 2 experiments). Error bars in all experiments, SD.

ns, non-significant. See also Tables S7, S8, and S9.

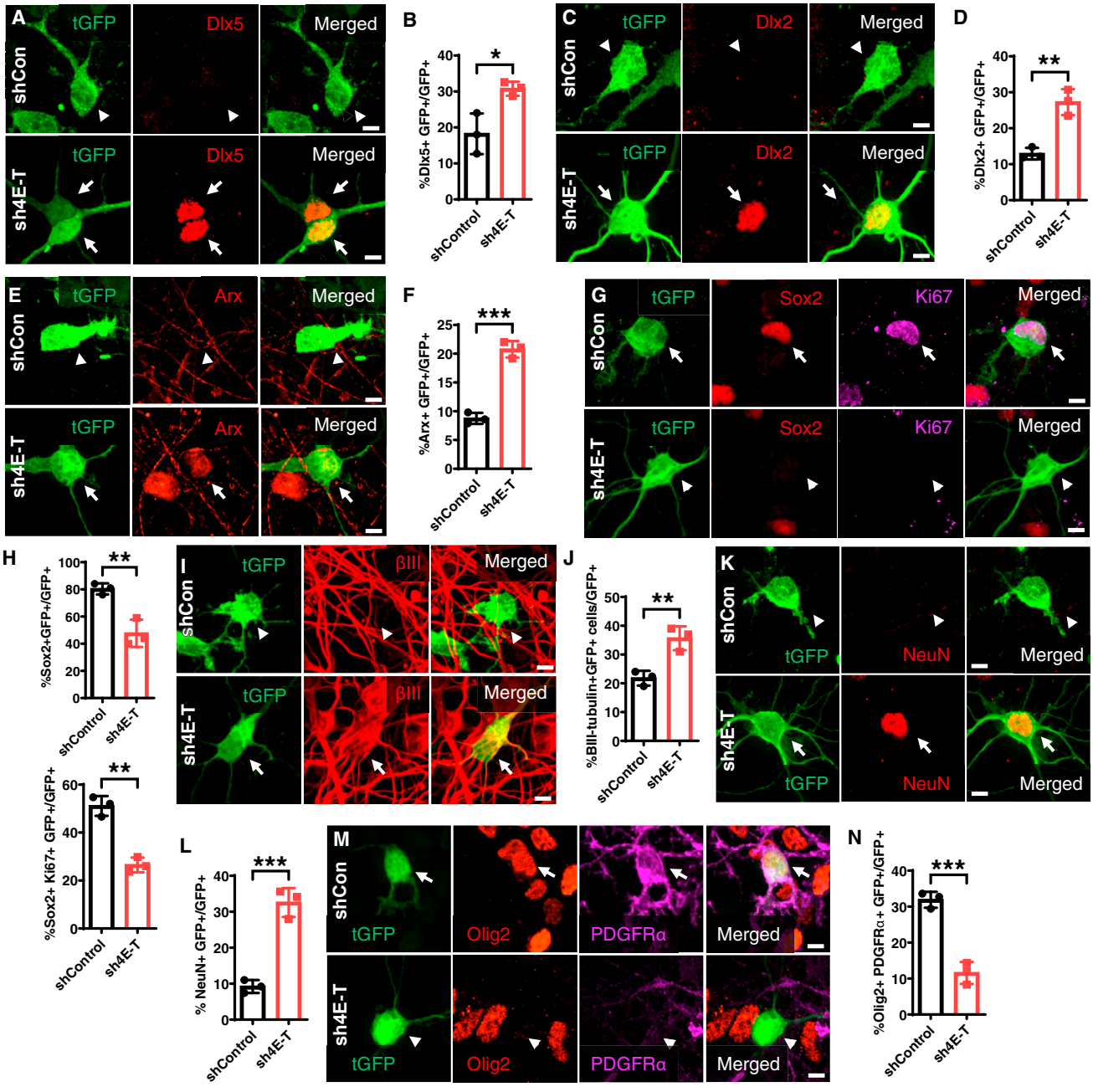

(legend on next page)

(Figures 7A and 7B). The total number of Sox2-positive, glial fibrillary acidic protein (GFAP)-positive NSCs and the total number of those that were Ki67 positive were also significantly decreased (Figures 7C–7E). This was not due to cell death because cleaved caspase-3-positive cells were similar in both groups (Figure 7F). As predicted, these changes were accompanied by decreased *4et* mRNA expression in Sox2-positive NPCs (Figure 7G). As a complementary approach, we cultured neurospheres from the V-SVZ of P7/8 *Nestin-CreERT2;4et*$^{fl/fl}$ and *4et*$^{fl/fl}$ littermates and after 5 days treated them with tamoxifen for 2–3 days. *Nestin-CreERT2;4et*$^{fl/fl}$ primary and secondary neurospheres were both significantly decreased relative to control *4et*$^{fl/fl}$ neurospheres (Figures 7H and 7I).

We asked whether loss of 4E-T derepressed proneurogenic mRNA translation *in vivo* as it did in culture, focusing on the 4E-T target Dlx2. *Nestin-CreERT2;4et*$^{fl/fl}$ and *4et*$^{fl/fl}$ littermates were treated with tamoxifen via their mother's milk from P1 to P3, and sections were immunostained at P8. The number of V-SVZ Dlx2 protein-positive cells was significantly increased following inducible knockout of *4et* (Figures 7J and 7K). To ask whether this derepression of Dlx2 translation was coincident with an increase in olfactory neurogenesis, we immunostained similar sections for Ctip2/Bcl11b, a transcription factor that was not a target of 4E-T in our RIP-seq analyses. We confirmed that Ctip2/Bcl11b is expressed in olfactory neuroblasts as it is in other forebrain interneurons[59] by (1) analysis of our scRNA-seq data (Figure S4A) and (2) immunostaining of olfactory neuroblasts in the RMS (Figure S4B). Analysis of P8 *Nestin-CreERT2;4et*$^{fl/fl}$ versus *4et*$^{fl/fl}$ sections demonstrated that inducible knockout of *4et* caused an almost 2-fold increase in the number of Ctip2-positive V-SVZ cells (Figure 7M). Thus, loss of 4E-T perturbed the balance between cell genesis and establishment of postnatal NSC pools, potentially by derepressing proneurogenic mRNAs such as *Dlx2*.

DISCUSSION

During the first 3 postnatal weeks, murine NPCs residing around the lateral ventricles must generate neurons and glia for forebrain development and at the same time establish adult NSC pools. Here, we show that this balance requires 4E-T-dependent translational repression of transcriptionally primed neonatal NPCs, and that when 4E-T is disrupted this causes aberrant differentiation and depletion of postnatal NSC pools. Why then are postnatal NPCs transcriptionally primed? One explanation is that mRNA transcription, processing, and targeting are relatively slow processes, whereas primed mRNAs could be quickly derepressed for rapid differentiation.[2,3,60,61] Transcriptional priming could also allow the same NPC to be ready to differentiate into diverse cell types. For example, V-SVZ NPCs generate oligodendrocytes and different interneuron subtypes as a function of their location,[9,62–64] and transcriptional priming could allow the local environment to rapidly select one cell type versus the other for differentiation. Thus, post-transcriptional mechanisms do not replace transcriptional regulation but instead provide an additional rapid and flexible layer on top of it.

Our data highlight the postnatal time period as a window of vulnerability both for cell genesis and for establishment of adult NSC pools. Further support for this idea comes from (1) recent scRNA-seq studies showing that the transition between highly active embryonic precursors and adult dormant NSCs occurs gradually over the first 2–3 postnatal weeks[12,65,66] and (2) work showing that an aberrant neonatal surge of interleukin-6 deregulated neonatal NPCs and ultimately caused depletion of the adult NSC pool,[67] findings reminiscent of the postnatal NSC depletion seen here with inducible 4E-T knockouts. Thus, key questions for the future are whether similar long-lasting NSC alterations occur in humans exposed to adverse pathological conditions as children and, if so, whether these have functional consequences.

One surprising finding reported here is that 4E-T preferentially associates with many mRNAs encoding transcriptional regulators. Why is this so? On one level, this makes biological sense, because these potent proteins presumably need to be very tightly regulated at multiple levels. However, it is not intuitive how this particular mRNA class is selected for 4E-T association, because 4E-T associates with mRNAs through interactions with RBPs such as Pumilio and Smaug.[5,7] Although this could indicate that the specificity comes from the RBPs, we previously showed that in the embryonic cortex, Pumilio2 associated with mRNAs encoding diverse types

Figure 6. 4E-T knockdown in perinatal cultures causes translational derepression and alters NPC maintenance and differentiation

(A–N) E15/16 cortical precursor cultures were co-transfected with PB transposase plasmid plus a PB vector encoding both turbo GFP (tGFP) and shRNA for 4E-T (sh4E-T) or luciferase (shControl) and analyzed 4.5 days later. (A, C, and E) Confocal images of cultures immunostained for tGFP (green) and Dlx5 (A, red), Dlx2 (C, red) or Arx (E, red). Arrows denote double-labeled cells, and arrowheads denote cells that are only tGFP positive. (B, D, and F) Scatterplots showing the percentage of tGFP-positive cells co-expressing Dlx5 (B), Dlx2 (D), or Arx (F) in cultures as in (A), (C), and (E). *$p < 0.05$, **$p < 0.01$, ***$p < 0.001$ ($n = 3$ experiments each). (G) Confocal images of cultures triple-labeled for Sox2 (red), Ki67 (magenta), and tGFP (green). Arrow denotes a triple-labeled cell, and arrowhead denotes a cell that is only tGFP positive. (H) Scatterplot showing percentage of tGFP-positive cells that coexpress Sox2 (top) or Sox2 and Ki67 (bottom) in cultures as in (G). **$p < 0.01$ ($n = 3$ experiments each). (I, K, and M) Confocal images of cultures immunostained for tGFP (green) and βIII-tubulin (I, red), NeuN (K, red), or Olig2 (M, red) and PDGFRα (magenta). Arrows indicate double- (I and K) or triple-labeled (M) cells, and arrowheads denote cells that are only tGFP positive. (J, L, and N) Scatterplots showing percentages of tGFP-positive cells that coexpress βIII-tubulin (J), NeuN (L), or both Olig2 and PDGFRα (N) in cultures as in (I), (K), and (M). **$p < 0.01$, ***$p < 0.005$ ($n = 3$ experiments each).

(O and P) Primary neurospheres generated from P7/8 *NestinCreERT2*$^{+/-}$*;4et*$^{fl/fl}$ (Cre$^+$) or *4et*$^{fl/fl}$ (Cre$^-$) littermates were cultured for 5 days and tamoxifen-treated for 2.5 additional days. (O) RT-PCR analysis of *4et* mRNA in Cre$^+$ and Cre$^-$ neurospheres from individual animals using primers spanning floxed exon 4. The arrow and arrowhead indicate the predicted 270- and 143-bp products deriving from the non-excised and excised floxed *4et* mRNAs. Size markers are on the left. Samples were also analyzed for *Rpl8* mRNA as a control (bottom). (P) Western blot of Cre$^+$ and Cre$^-$ neurosphere lysates from individual animals probed for 4E-T (top, arrow) and reprobed for ERK1/2 (bottom) as a loading control. Molecular weight markers are on the left.

(Q) Western blot of neurospheres cultured from the P7/8 V-SVZ of a *NestinCreERT2*$^{+/-}$*;4et*$^{fl/fl}$ mouse for 5 days and treated with tamoxifen (Tamox.) or the DMSO vehicle (DMSO) for an additional 2.5 days, probed for 4E-T (top, arrow) and reprobed for ERK1/2 (bottom). Molecular weight markers are on the left. Error bars indicate SD in all experiments. Scale bars, 5 μm.

See also Figures S2 and S3.

CellPress
OPEN ACCESS

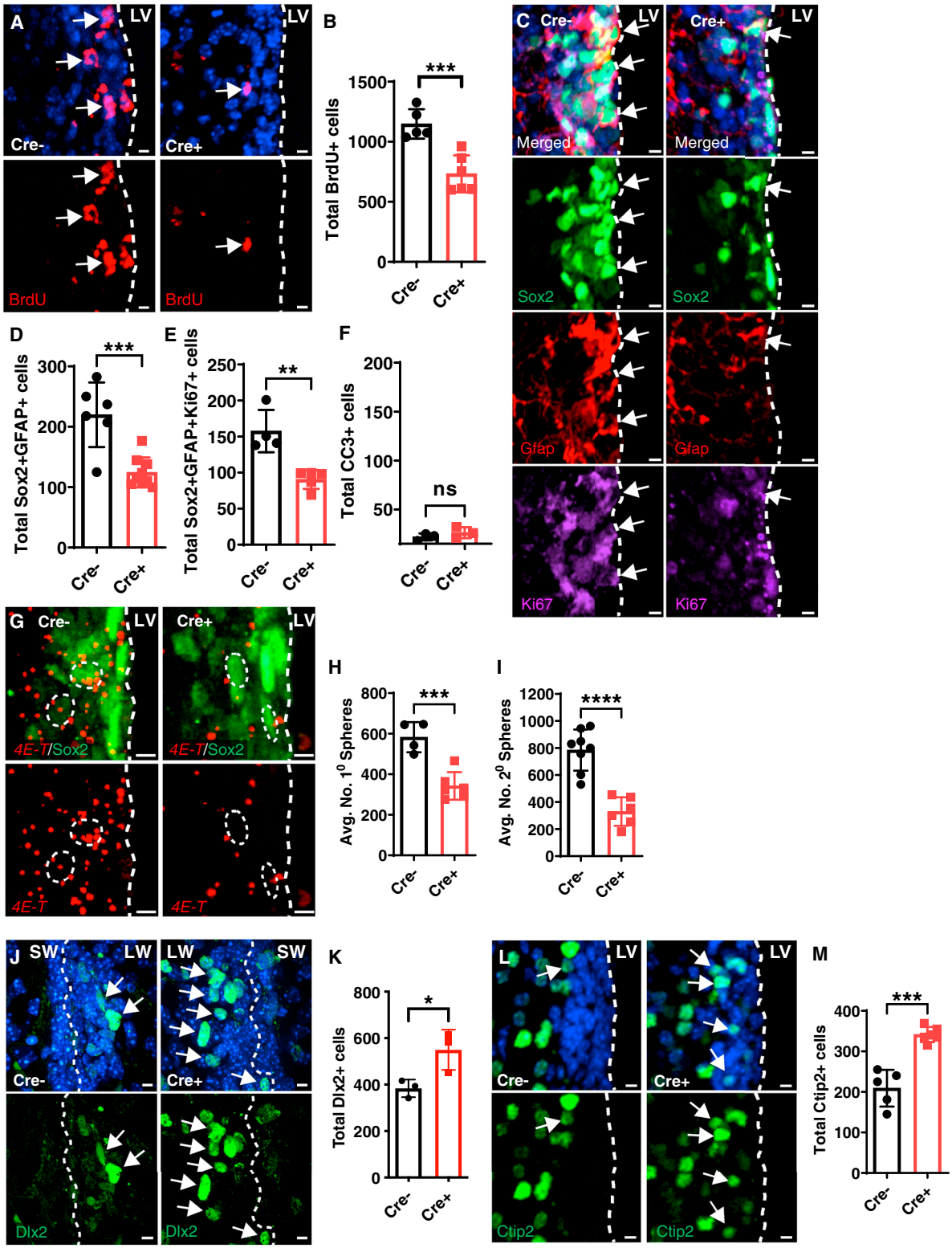

Figure 7. 4E-T ablation *in vivo* perturbs NPC maintenance and differentiation

(A–G) *NestinCreERT2*$^{+/-}$;*4et*$^{fl/fl}$ (Cre^{+}) or *4et*$^{fl/fl}$ (Cre^{-}) neonatal mice were exposed to tamoxifen via mother's milk at P1–P3, and the lateral V-SVZ was analyzed at P8. Some mice also received BrdU at P7. (A) Representative BrdU immunostaining (red) images of the Cre^{+} or Cre^{-} V-SVZ. Arrows indicate BrdU-positive cells.

(legend continued on next page)

of proteins but that the shared Pumilio2/4E-T targets were enriched for mRNAs encoding transcriptional regulators.[7] Thus, it may be that 4E-T and/or perhaps other associated P-body proteins (see discussion below) somehow recognize and associate specifically with RBPs bound to mRNAs encoding regulatory proteins.

How then does 4E-T repress translation of its associated mRNAs? Our data show that 4E-T localizes to P-bodies in NPCs as it does in other cells.[41,68] P-bodies are dynamic granules composed of repressive mRNA-ribonucleoprotein complexes that arise by liquid-liquid phase separation. Notably, P-body-targeted mRNAs have a low translation rate and encode proteins with regulatory functions[16,17,38] similar to what we have seen for 4E-T-associated mRNAs in NPCs. Within P-bodies, 4E-T is known to nucleate multiple P-body proteins[42,69–74] and to interact with Tnrc6b to direct the deadenylation complex CCR4-NOT to store target mRNAs in a silenced, deadenylated, and undegraded form.[69] 4E-T can also bind to eIF4E and competitively sequester it from eIF4G, thereby impeding translational initiation,[70,75,76] a mechanism we showed is important in embryonic NPCs.[6] Thus, we posit that 4E-T targets RBPs associated with mRNAs encoding transcriptional regulators to P-bodies and in so doing sequesters them in a repressed state away from polysomes.

Our findings indicate that the situation is very different for Cpeb4, which can both repress and activate translation.[21] For example, in late meiosis of oocytes, Cpeb4 promotes formation of the initiation complex and subsequent translation of previously silenced mRNAs.[21,77,78] By contrast, during terminal erythropoiesis, Cpeb4 interacts with eIF3 to repress translation.[19] Cpeb4 is also clearly important during brain development, as exemplified by a study implicating alterations in Cpeb4 splicing in idiopathic ASD[23] and by data presented here. However, our findings suggest that Cpeb4 may be more important for translational activation than for repression because Cpeb4 binds mRNAs encoding diverse categories of proteins in neonatal NPCs, and many of these are ribosome associated. Nonetheless, ribosome association does not definitively indicate mRNA translation, and it is still possible that Cpeb4 associates with mRNAs on stalled ribosomes, as has been seen for FMRP.[79]

Together, our studies shed light on cellular mechanisms that regulate postnatal NPCs during a key developmental window and support a model where neonatal NPCs are transcriptionally primed for differentiation and where 4E-T maintains the balance between cell genesis and establishment of the NSC pool by sequestering and repressing mRNAs encoding transcriptional regulators.

Limitations of the study

There are several technical limitations of this study. First, it is difficult to isolate sufficient V-SVZ NPCs for the biochemical/molecular analyses presented here, and we instead used NPCs cultured and expanded as neurospheres. Nonetheless, we addressed this limitation, at least in part, by performing complementary experiments in primary cultured cortical precursors and *in vivo* in the mouse. Second, although we used both the RiboTag mouse line and polysome profiling for our ribosome association experiments, polysomal association does not guarantee that mRNAs are being translated. Nonetheless, our RiboTag studies show that the relative proportions of target mRNAs in the "ribosome-associated" and "ribosome-depleted" categories were very different for 4E-T and Cpeb4, thereby supporting the idea that many 4E-T target mRNAs are sequestered from polysomes and repressed. Finally, we did not want to overstate the conclusions drawn from analysis of the large datasets presented here, and we defined arbitrary cutoffs based on fold-change from controls. It is thus possible we are under-estimating the number of bona fide 4E-T and Cpeb4 target mRNAs.

STAR★METHODS

Detailed methods are provided in the online version of this paper and include the following:

- KEY RESOURCES TABLE
- RESOURCE AVAILABILITY
  - Lead contact
  - Materials availability
  - Data and code availability
- EXPERIMENTAL MODEL AND SUBJECT DETAILS
  - Mice
- METHOD DETAILS
  - BrdU and tamoxifen administration
  - Cell cultures and transfections
  - Stable knockdown plasmid generation
  - Tissue preparation and immunostaining
  - Antibodies
  - Fluorescent *in situ* hybridization (FISH)
  - Imaging, microscopy and quantifications

(B) Scatterplot of total BrdU-positive cells in sections as in (A). ***$p < 0.001$ ($n = 5$ Cre^- and 6 Cre^+ animals). (C) Representative images of V-SVZ sections as in (A), immunostained for Sox2 (green), GFAP (red), and Ki67 (violet). Arrows denote triple-positive cells. (D and E) Scatterplots of sections as in (C) analyzed for Sox2 and GFAP double-positive cells (D) or Sox2-positive, GFAP-positive, Ki67-positive triple-labeled cells (E). **$p < 0.01$, ***$p < 0.005$ ($n = 4–6$ Cre^- and 5–8 Cre^+ animals). (F) Scatterplot of sections as in (A) that were immunostained and quantified for cleaved caspase-3 (CC3)-positive cells. ns, non-significant ($n = 3$ animals each). (G) Representative images of the P8 Cre^- and Cre^+ V-SVZ analyzed for *4et* mRNA (red) by FISH and immunostained for Sox2 protein (green). Select nuclei are outlined with hatched white ovals.

(H and I) Scatterplots of V-SVZ neurospheres from P7/8 *NestinCreERT2*$^{+/-}$*;4et*$^{fl/fl}$ (Cre^+) or *4et*$^{fl/fl}$ (Cre^-) mice that were cultured for 5 days and tamoxifen-treated for an additional 2 days. Primary neurospheres were quantified (H) or were passaged at equal cell densities, cultured as secondary neurospheres for 7–8 days more, and quantified (I). ***$p < 0.001$, ****$p < 0.0001$ ($n = 4–8$ Cre^- and 6 Cre^+ animals).

(J and L) Representative images of V-SVZ sections as in (A), immunostained for Dlx2 (J, green) or Ctip2 (L, green).

(K and M) Scatterplots of sections as in (J) and (L) analyzed for total Dlx2-positive (K) or Ctip2-positive (M) cells. *$p < 0.05$, ***$p < 0.001$ ($n = 3–5$ Cre^- and 3–6 Cre^+ animals).

In all images, the LV or LW boundary is denoted with a hatched line. Error bars, SD in all experiments. Scale bars, 5 μm. In (A), (C), (J), and (L), sections were counterstained for Hoechst 33258 (blue). SW, septal wall. See also Figure S4.

- Neurosphere cultures
- Western blotting
- Immunoprecipitation
- RNA immunoprecipitation sequencing (RIP-seq)
- RiboTag analysis
- Microarray analysis
- Polysome fractionation and profiling
- Real-time quantitative PCR
- scRNA-seq analysis

- QUANTIFICATION AND STATISTICAL ANALYSIS
  - Quantification of RiboTag experiments
  - Quantification of marker-positive cells in 4E-T ablation *in vivo* experiments
  - Quantification of marker-positive cells in 4E-T knockdown *in vitro* experiments
  - Quantification of marker-positive cells in the perinatal and adult V-SVZ
  - Statistical analysis

SUPPLEMENTAL INFORMATION

Supplemental information can be found online at https://doi.org/10.1016/j.celrep.2023.112242.

ACKNOWLEDGMENTS

This work was supported by an RNA and the Brain grant from the Azrieli Foundation (to D.R.K., F.D.M., and G.Y.), NSERC (to G.Y.), and CIHR (to F.D.M. and D.R.K.). We thank Denis Gallagher for generating the P8 neurosphere microarray data and Nareh Tahmasian for her help with establishing the perinatal cortical cultures. We also thank Dina McRae for her input and guidance on the scRNA-seq analyses, SickKids TCAG facility for their help with the analysis of the RIP-seq experiments, and Sarah Burns and Jasmine Yang for invaluable technical assistance.

AUTHOR CONTRIBUTIONS

A.K. conceptualized, performed, and analyzed most of the experiments and co-wrote the paper. S.K.Z. and G.Y. generated the *4et*$^{fl/fl}$ mouse model, and S.K.Z. conceptualized, performed, and analyzed most of the *in vivo* mouse data. B.S.W. worked with A.K. to establish the perinatal cortical culture system and participated in revising the manuscript. T.K. worked with A.K. to perform the polysome profiling studies, and H.K. provided essential input on the computational analyses. S.K.Z., G.Y., and B.S.W. all provided input on the manuscript. F.D.M. and D.R.K. conceptualized experiments, analyzed data, and co-wrote the paper.

DECLARATION OF INTERESTS

The authors declare no competing interests.

INCLUSION AND DIVERSITY

We support inclusive, diverse, and equitable conduct of research.

Received: August 25, 2022
Revised: January 19, 2023
Accepted: February 23, 2023
Published: March 15, 2023

REFERENCES

1. DeBoer, E.M., Kraushar, M.L., Hart, R.P., and Rasin, M.-R. (2013). Post-transcriptional regulatory elements and spatiotemporal specification of neocortical stem cells and projection neurons. Neuroscience *248*, 499–528.
2. Tahmasebi, S., Amiri, M., and Sonenberg, N. (2018). Translational control in stem cells. Front. Genet. *9*, 709.
3. Teixeira, F.K., and Lehmann, R. (2019). Translational control during developmental transitions. Cold Spring Harb. Perspect. Biol. *11*, a032987.
4. Zahr, S.K., Kaplan, D.R., and Miller, F.D. (2019). Translating neural stem cells to neurons in the mammalian brain. Cell Death Differ. *26*, 2495–2512.
5. Amadei, G., Zander, M.A., Yang, G., Dumelie, J.G., Vessey, J.P., Lipshitz, H.D., Smibert, C.A., Kaplan, D.R., and Miller, F.D. (2015). A Smaug2-based translational repression complex determines the balance between precursor maintenance versus differentiation during mammalian neurogenesis. J. Neurosci. *35*, 15666–15681.
6. Yang, G., Smibert, C.A., Kaplan, D.R., and Miller, F.D. (2014). An eIF4E1/4E-T complex determines the genesis of neurons from precursors by translationally repressing a proneurogenic transcription program. Neuron *84*, 723–739.
7. Zahr, S.K., Yang, G., Kazan, H., Borrett, M.J., Yuzwa, S.A., Voronova, A., Kaplan, D.R., and Miller, F.D. (2018). A translational repression complex in developing mammalian neural stem cells that regulates neuronal specification. Neuron *97*, 520–537.e6.
8. Lim, D.A., and Alvarez-Buylla, A. (2016). The adult ventricular–subventricular zone (V-SVZ) and olfactory bulb (OB) neurogenesis. Cold Spring Harb. Perspect. Biol. *8*, a018820.
9. Menn, B., Garcia-Verdugo, J.M., Yaschine, C., Gonzalez-Perez, O., Rowitch, D., and Alvarez-Buylla, A. (2006). Origin of oligodendrocytes in the subventricular zone of the adult brain. J. Neurosci. *26*, 7907–7918.
10. Fuentealba, L.C., Rompani, S.B., Parraguez, J.I., Obernier, K., Romero, R., Cepko, C.L., and Alvarez-Buylla, A. (2015). Embryonic origin of postnatal neural stem cells. Cell *161*, 1644–1655.
11. Furutachi, S., Miya, H., Watanabe, T., Kawai, H., Yamasaki, N., Harada, Y., Imayoshi, I., Nelson, M., Nakayama, K.I., Hirabayashi, Y., and Gotoh, Y. (2015). Slowly dividing neural progenitors are an embryonic origin of adult neural stem cells. Nat. Neurosci. *18*, 657–665.
12. Yuzwa, S.A., Borrett, M.J., Innes, B.T., Voronova, A., Ketela, T., Kaplan, D.R., Bader, G.D., and Miller, F.D. (2017). Developmental emergence of adult neural stem cells as revealed by single-cell transcriptional profiling. Cell Rep. *21*, 3970–3986.
13. Rajman, M., and Schratt, G. (2017). MicroRNAs in neural development: from master regulators to fine-tuners. Development *144*, 2310–2322.
14. Sun, G., Ye, P., Murai, K., Lang, M.-F., Li, S., Zhang, H., Li, W., Fu, C., Yin, J., Wang, A., et al. (2011). miR-137 forms a regulatory loop with nuclear receptor TLX and LSD1 in neural stem cells. Nat. Commun. *2*, 529.
15. Zhao, C., Sun, G., Li, S., and Shi, Y. (2009). A feedback regulatory loop involving microRNA-9 and nuclear receptor TLX in neural stem cell fate determination. Nat. Struct. Mol. Biol. *16*, 365–371.
16. Ivanov, P., Kedersha, N., and Anderson, P. (2019). Stress granules and processing bodies in translational control. Cold Spring Harb. Perspect. Biol. *11*, a032813.
17. Standart, N., and Weil, D. (2018). P-Bodies: Cytosolic droplets for coordinated mRNA storage. Trends Genet. *34*, 612–626.
18. Hake, L.E., and Richter, J.D. (1994). CPEB is a specificity factor that mediates cytoplasmic polyadenylation during Xenopus oocyte maturation. Cell *79*, 617–627.
19. Hu, W., Yuan, B., and Lodish, H.F. (2014). Cpeb4-mediated translational regulatory circuitry controls terminal erythroid differentiation. Dev. Cell *30*, 660–672.
20. Huang, Y.-S., Kan, M.-C., Lin, C.-L., and Richter, J.D. (2006). CPEB3 and CPEB4 in neurons: Analysis of RNA-binding specificity and translational control of AMPA receptor GluR2 mRNA. EMBO J. *25*, 4865–4876.
21. Kozlov, E., Shidlovskii, Y.V., Gilmutdinov, R., Schedl, P., and Zhukova, M. (2021). The role of CPEB family proteins in the nervous system function in the norm and pathology. Cell Biosci. *11*, 64.

22. Ortiz-Zapater, E., Pineda, D., Martínez-Bosch, N., Fernández-Miranda, G., Iglesias, M., Alameda, F., Moreno, M., Eliscovich, C., Eyras, E., Real, F.X., et al. (2011). Key contribution of CPEB4-mediated translational control to cancer progression. Nat. Med. *18*, 83–90.

23. Parras, A., Anta, H., Santos-Galindo, M., Swarup, V., Elorza, A., Nieto-González, J.L., Picó, S., Hernández, I.H., Díaz-Hernández, J.I., Belloc, E., et al. (2018). Autism-like phenotype and risk gene mRNA deadenylation by CPEB4 mis-splicing. Nature *560*, 441–446.

24. Allen, Z.J., Waclaw, R.R., Colbert, M.C., and Campbell, K. (2007). Molecular identity of olfactory bulb interneurons: transcriptional codes of periglomerular neuron subtypes. J. Mol. Histol. *38*, 517–525.

25. Brill, M.S., Snapyan, M., Wohlfrom, H., Ninkovic, J., Jawerka, M., Mastick, G.S., Ashery-Padan, R., Saghatelyan, A., Berninger, B., and Götz, M. (2008). A Dlx2- and Pax6-dependent transcriptional code for periglomerular neuron specification in the adult olfactory bulb. J. Neurosci. *28*, 6439–6452.

26. Colasante, G., Collombat, P., Raimondi, V., Bonanomi, D., Ferrai, C., Maira, M., Yoshikawa, K., Mansouri, A., Valtorta, F., Rubenstein, J.L.R., and Broccoli, V. (2008). Arx is a direct target of Dlx2 and thereby contributes to the tangential migration of GABAergic interneurons. J. Neurosci. *28*, 10674–10686.

27. Díaz-Guerra, E., Pignatelli, J., Nieto-Estévez, V., and Vicario-Abejón, C. (2019). Transcriptional regulation of olfactory bulb neurogenesis. Anat. Rec. *296*, 1364–1382.

28. Guo, T., Liu, G., Du, H., Wen, Y., Wei, S., Li, Z., Tao, G., Shang, Z., Song, X., Zhang, Z., et al. (2019). Dlx1/2 are central and essential components in the transcriptional code for generating olfactory bulb interneurons. Cereb. Cortex *29*, 4831–4849.

29. Kohwi, M., Petryniak, M.A., Long, J.E., Ekker, M., Obata, K., Yanagawa, Y., Rubenstein, J.L.R., and Alvarez-Buylla, A. (2007). A subpopulation of olfactory bulb GABAergic interneurons is derived from Emx1- and Dlx5/6-expressing progenitors. J. Neurosci. *27*, 6878–6891.

30. Levi, G., Puche, A.C., Mantero, S., Barbieri, O., Trombino, S., Paleari, L., Egeo, A., and Merlo, G.R. (2003). The Dlx2 homeodomain gene is essential for olfactory development and connectivity in the mouse. Mol. Cell. Neurosci. *22*, 530–543.

31. Li, J., Wang, C., Zhang, Z., Wen, Y., An, L., Liang, Q., Xu, Z., Wei, S., Li, W., Guo, T., et al. (2018). Transcription factors Sp8 and Sp9 coordinately regulate olfactory bulb interneuron development. Cereb. Cortex *28*, 3278–3294.

32. Waclaw, R.R., Allen, Z.J., Bell, S.M., Erdélyi, F., Szabó, G., Potter, S.S., and Campbell, K. (2006). The zinc finger transcription factor Sp8 regulates the generation and diversity of olfactory bulb interneurons. Neuron *49*, 503–516.

33. Yoshihara, S.i., Omichi, K., Yanazawa, M., Kitamura, K., and Yoshihara, Y. (2005). Arx homeobox gene is essential for development of mouse olfactory system. Development *132*, 751–762.

34. Cebrian-Silla, A., Nascimento, M.A., Redmond, S.A., Mansky, B., Wu, D., Obernier, K., Romero Rodriguez, R., Gonzalez-Granero, S., García-Verdugo, J.M., Lim, D.A., and Álvarez-Buylla, A. (2021). Single-cell analysis of the ventricular-subventricular zone reveals signatures of dorsal and ventral adult neurogenesis. Elife *10*, e67436.

35. Kim, E.J., Leung, C.T., Reed, R.R., and Johnson, J.E. (2007). In vivo analysis of Ascl1 defined progenitors reveals distinct developmental dynamics during adult neurogenesis and gliogenesis. J. Neurosci. *27*, 12764–12774.

36. Mizrak, D., Levitin, H.M., Delgado, A.C., Crotet, V., Yuan, J., Chaker, Z., Silva-Vargas, V., Sims, P.A., and Doetsch, F. (2019). Single-cell analysis of regional differences in adult V-SVZ neural stem cell lineages. Cell Rep. *26*, 394–406.e5.

37. Pastrana, E., Cheng, L.-C., and Doetsch, F. (2009). Simultaneous prospective purification of adult subventricular zone neural stem cells and their progeny. Proc. Natl. Acad. Sci. USA *106*, 6387–6392.

38. Hubstenberger, A., Courel, M., Bénard, M., Souquere, S., Ernoult-Lange, M., Chouaib, R., Yi, Z., Morlot, J.-B., Munier, A., Fradet, M., et al. (2017). P-body purification reveals the condensation of repressed mRNA regulons. Mol. Cell *68*, 144–157.e5.

39. Minshall, N., Kress, M., Weil, D., and Standart, N. (2009). Role of p54 RNA helicase activity and its C-terminal domain in translational repression, P-body localization and assembly. Mol. Biol. Cell *20*, 2464–2472.

40. Youn, J.-Y., Dunham, W.H., Hong, S.J., Knight, J.D.R., Bashkurov, M., Chen, G.I., Bagci, H., Rathod, B., MacLeod, G., Eng, S.W.M., et al. (2018). High-density proximity mapping reveals the subcellular organization of mRNA-associated granules and bodies. Mol. Cell *69*, 517–532.e11.

41. Ferraiuolo, M.A., Basak, S., Dostie, J., Murray, E.L., Schoenberg, D.R., and Sonenberg, N. (2005). A role for the eIF4E-binding protein 4E-T in P-body formation and mRNA decay. J. Cell Biol. *170*, 913–924.

42. Kamenska, A., Simpson, C., Vindry, C., Broomhead, H., Bénard, M., Ernoult-Lange, M., Lee, B.P., Harries, L.W., Weil, D., and Standart, N. (2016). The DDX6–4E-T interaction mediates translational repression and P-body assembly. Nucleic Acids Res. *44*, 6318–6334.

43. Cubelos, B., Sebastián-Serrano, A., Kim, S., Redondo, J.M., Walsh, C., and Nieto, M. (2008). Cux-1 and Cux-2 control the development of Reelin expressing cortical interneurons. Dev. Neurobiol. *68*, 917–925.

44. Shen, W., Ba, R., Su, Y., Ni, Y., Chen, D., Xie, W., Pleasure, S.J., and Zhao, C. (2019). Foxg1 regulates the postnatal development of cortical interneurons. Cereb. Cortex *29*, 1547–1560.

45. Shepard, R., Heslin, K., Hagerdorn, P., and Coutellier, L. (2019). Downregulation of Npas4 in parvalbumin interneurons and cognitive deficits after neonatal NMDA receptor blockade: relevance for schizophrenia. Transl. Psychiatry *9*. 99–11.

46. Waclaw, R.R., Wang, B., Pei, Z., Ehrman, L.A., and Campbell, K. (2009). Distinct temporal requirements for the homeobox gene Gsx2 in specifying striatal and olfactory bulb neuronal fates. Neuron *63*, 451–465.

47. Yoshihara, S.-I., Takahashi, H., Nishimura, N., Kinoshita, M., Asahina, R., Kitsuki, M., Tatsumi, K., Furukawa-Hibi, Y., Hirai, H., Nagai, T., et al. (2014). Npas4 regulates Mdm2 and thus Dcx in experience-dependent dendritic spine development of newborn olfactory bulb interneurons. Cell Rep. *8*, 843–857.

48. Pozniak, C.D., Langseth, A.J., Dijkgraaf, G.J.P., Choe, Y., Werb, Z., and Pleasure, S.J. (2010). Sox10 directs neural stem cells toward the oligodendrocyte lineage by decreasing Suppressor of Fused expression. Proc. Natl. Acad. Sci. USA *107*, 21795–21800.

49. Stevanovic, M., Drakulic, D., Lazic, A., Ninkovic, D.S., Schwirtlich, M., and Mojsin, M. (2021). SOX transcription factors as important regulators of neuronal and glial differentiation during nervous system development and adult neurogenesis. Front. Mol. Neurosci. *14*, 654031.

50. Wegner, M. (2008). A matter of identity: Transcriptional control in oligodendrocytes. J. Mol. Neurosci. *35*, 3–12.

51. Imayoshi, I., Ohtsuka, T., Metzger, D., Chambon, P., and Kageyama, R. (2006). Temporal regulation of Cre recombinase activity in neural stem cells. Genesis *44*, 233–238.

52. Baser, A., Skabkin, M., Kleber, S., Dang, Y., Gülcüler Balta, G.S., Kalamakis, G., Göpferich, M., Ibañez, D.C., Schefzik, R., Lopez, A.S., et al. (2019). Onset of differentiation is post-transcriptionally controlled in adult neural stem cells. Nature *566*, 100–104.

53. Lesiak, A.J., Brodsky, M., and Neumaier, J.F. (2015). RiboTag is a flexible tool for measuring the translational state of targeted cells in heterogeneous cell cultures. Biotechniques *58*, 308–317.

54. Sanz, E., Bean, J.C., Carey, D.P., Quintana, A., and McKnight, G.S. (2019). RiboTag: ribosomal tagging strategy to analyze cell-type-specific mRNA expression in vivo. Curr. Protoc. Neurosci. *88*, e77.

55. Kedia, S., Erickson, S.L., and Yang, G. (2021). Analysis of translation in the developing mouse brain using polysome profiling. J. Vis. Exp. https://doi.org/10.3791/62088.

56. Skarnes, W.C., Rosen, B., West, A.P., Koutsourakis, M., Bushell, W., Iyer, V., Mujica, A.O., Thomas, M., Harrow, J., Cox, T., et al. (2011). A conditional knockout resource for the genome-wide study of mouse gene function. Nature *474*, 337–342.

57. Testa, G., Schaft, J., van der Hoeven, F., Glaser, S., Anastassiadis, K., Zhang, Y., Hermann, T., Stremmel, W., and Stewart, A.F. (2004). A reliable lacZ expression reporter cassette for multipurpose, knockout-first alleles. genesis *38*, 151–158.

58. Wu, Y., Wang, C., Sun, H., LeRoith, D., and Yakar, S. (2009). High-efficient FLPo deleter mice in C57BL/6J background. PLoS One *4*, e8054.

59. Nikouei, K., Muñoz-Manchado, A.B., and Hjerling-Leffler, J. (2016). BCL11B/CTIP2 is highly expressed in GABAergic interneurons of the mouse somatosensory cortex. J. Chem. Neuroanat. *71*, 1–5.

60. Joshi, A., Beck, Y., and Michoel, T. (2012). Post-transcriptional regulatory networks play a key role in noise reduction that is conserved from micro-organisms to mammals. FEBS J. *279*, 3501–3512.

61. Liu, Y., Beyer, A., and Aebersold, R. (2016). On the dependency of cellular protein levels on mRNA abundance. Cell *165*, 535–550.

62. Hack, M.A., Saghatelyan, A., de Chevigny, A., Pfeifer, A., Ashery-Padan, R., Lledo, P.-M., and Götz, M. (2005). Neuronal fate determinants of adult olfactory bulb neurogenesis. Nat. Neurosci. *8*, 865–872.

63. Merkle, F.T., Mirzadeh, Z., and Alvarez-Buylla, A. (2007). Mosaic organization of neural stem cells in the adult brain. Science *317*, 381–384.

64. Tong, C.K., Fuentealba, L.C., Shah, J.K., Lindquist, R.A., Ihrie, R.A., Guinto, C.D., Rodas-Rodriguez, J.L., and Alvarez-Buylla, A. (2015). A dorsal SHH-dependent domain in the V-SVZ produces large numbers of oligodendroglial lineage cells in the postnatal brain. Stem Cell Rep. *5*, 461–470.

65. Borrett, M.J., Innes, B.T., Tahmasian, N., Bader, G.D., Kaplan, D.R., and Miller, F.D. (2022). A shared transcriptional identity for forebrain and dentate gyrus neural stem cells from embryogenesis to adulthood. eNeuro *9*. ENEURO.0271-21.2021.

66. Borrett, M.J., Innes, B.T., Jeong, D., Tahmasian, N., Storer, M.A., Bader, G.D., Kaplan, D.R., and Miller, F.D. (2020). Single-cell profiling shows murine forebrain neural stem cells reacquire a developmental state when activated for adult neurogenesis. Cell Rep. *32*, 108022.

67. Storer, M.A., Gallagher, D., Fatt, M.P., Simonetta, J.V., Kaplan, D.R., and Miller, F.D. (2018). Interleukin-6 regulates adult neural stem cell numbers during normal and abnormal post-natal development. Stem Cell Rep. *10*, 1464–1480.

68. Andrei, M.A., Ingelfinger, D., Heintzmann, R., Achsel, T., Rivera-Pomar, R., and Lührmann, R. (2005). A role for eIF4E and eIF4E-transporter in targeting mRNPs to mammalian processing bodies. RNA *11*, 717–727.

69. Räsch, F., Weber, R., Izaurralde, E., and Igreja, C. (2020). 4E-T-bound mRNAs are stored in a silenced and deadenylated form. Genes Dev. *34*, 847–860.

70. Mader, S., Lee, H., Pause, A., and Sonenberg, N. (1995). The translation initiation factor eIF-4E binds to a common motif shared by the translation factor eIF-4 gamma and the translational repressors 4E-binding proteins. Mol. Cell Biol. *15*, 4990–4997.

71. Kamenska, A., Lu, W.-T., Kubacka, D., Broomhead, H., Minshall, N., Bushell, M., and Standart, N. (2014). Human 4E-T represses translation of bound mRNAs and enhances microRNA-mediated silencing. Nucleic Acids Res. *42*, 3298–3313.

72. Nishimura, T., Padamsi, Z., Fakim, H., Milette, S., Dunham, W.H., Gingras, A.-C., and Fabian, M.R. (2015). The eIF4E-binding protein 4E-T is a component of the mRNA decay machinery that bridges the 5' and 3' termini of target mRNAs. Cell Rep. *11*, 1425–1436.

73. Ozgur, S., Basquin, J., Kamenska, A., Filipowicz, W., Standart, N., and Conti, E. (2015). Structure of a human 4E-T/DDX6/CNOT1 complex reveals the different interplay of DDX6-binding proteins with the CCR4-NOT complex. Cell Rep. *13*, 703–711.

74. Brandmann, T., Fakim, H., Padamsi, Z., Youn, J.-Y., Gingras, A.-C., Fabian, M.R., and Jinek, M. (2018). Molecular architecture of LSM14 interactions involved in the assembly of mRNA silencing complexes. EMBO J. *37*, e97869.

75. Peter, D., Igreja, C., Weber, R., Wohlbold, L., Weiler, C., Ebertsch, L., Weichenrieder, O., and Izaurralde, E. (2015). Molecular architecture of 4E-BP translational inhibitors bound to eIF4E. Mol. Cell *57*, 1074–1087.

76. Grüner, S., Weber, R., Peter, D., Chung, M.-Y., Igreja, C., Valkov, E., and Izaurralde, E. (2018). Structural motifs in eIF4G and 4E-BPs modulate their binding to eIF4E to regulate translation initiation in yeast. Nucleic Acids Res. *46*, 6893–6908.

77. Igea, A., and Méndez, R. (2010). Meiosis requires a translational positive loop where CPEB1 ensues its replacement by CPEB4. EMBO J. *29*, 2182–2193.

78. Guillén-Boixet, J., Buzon, V., Salvatella, X., and Méndez, R. (2016). CPEB4 is regulated during cell cycle by ERK2/Cdk1-mediated phosphorylation and its assembly into liquid-like droplets. Elife *5*, e19298.

79. Shah, S., Molinaro, G., Liu, B., Wang, R., Huber, K.M., and Richter, J.D. (2020). FMRP control of ribosome translocation promotes chromatin modifications and alternative splicing of neuronal genes linked to autism. Cell Rep. *30*, 4459–4472.e6.

80. Sanz, E., Yang, L., Su, T., Morris, D.R., McKnight, G.S., and Amieux, P.S. (2009). Cell-type-specific isolation of ribosome-associated mRNA from complex tissues. Proc. Natl. Acad. Sci. USA *106*, 13939–13944.

81. Voronova, A., Yuzwa, S.A., Wang, B.S., Zahr, S., Syal, C., Wang, J., Kaplan, D.R., and Miller, F.D. (2017). Migrating interneurons secrete fractalkine to promote oligodendrocyte formation in the developing mammalian brain. Neuron *94*, 500–516.e9.

82. Yuzwa, S.A., Yang, G., Borrett, M.J., Clarke, G., Cancino, G.I., Zahr, S.K., Zandstra, P.W., Kaplan, D.R., and Miller, F.D. (2016). Proneurogenic ligands defined by modeling developing cortex growth factor communication networks. Neuron *91*, 988–1004.

83. Jeong, D., Lozano Casasbuenas, D., Gengatharan, A., Edwards, K., Saghatelyan, A., Kaplan, D.R., Miller, F.D., and Yuzwa, S.A. (2020). LRIG1-mediated inhibition of EGF receptor signaling regulates neural precursor cell proliferation in the neocortex. Cell Rep. *33*, 108257.

84. Mi, H., Muruganujan, A., and Thomas, P.D. (2013). PANTHER in 2013: Modeling the evolution of gene function, and other gene attributes, in the context of phylogenetic trees. Nucleic Acids Res. *41*, D377–D386.

85. Reimand, J., Isserlin, R., Voisin, V., Kucera, M., Tannus-Lopes, C., Rostamianfar, A., Wadi, L., Meyer, M., Wong, J., Xu, C., et al. (2019). Pathway enrichment analysis and visualization of omics data using g:Profiler, GSEA, Cytoscape and EnrichmentMap. Nat. Protoc. *14*, 482–517.

86. Reimand, J., Kull, M., Peterson, H., Hansen, J., and Vilo, J. (2007). g:Profiler–a web-based toolset for functional profiling of gene lists from large-scale experiments. Nucleic Acids Res. *35*, W193–W200.

87. Love, M.I., Huber, W., and Anders, S. (2014). Moderated estimation of fold change and dispersion for RNA-seq data with DESeq2. Genome Biol. *15*, 550.

STAR★METHODS

KEY RESOURCES TABLE

REAGENT or RESOURCE	SOURCE	IDENTIFIER
Antibodies		
Mouse monoclonal anti-Ki67	BD Pharmingen	Cat# 550609; RRID: AB_393778
Mouse monoclonal anti-Dlx2 (B-5)	Santa Cruz	Cat# sc-393879
Mouse monoclonal anti-Olig2	EMD Millipore	Cat# Mabn50; RRID: AB_10807410
Rat monoclonal anti-Ctip2	Abcam	Cat# ab18465; RRID: AB_2064130
Rabbit polyclonal anti-βIII Tubulin	BioLegend	Cat# 802001; RRID: AB_2564645
Rat monoclonal anti-BrdU	Abcam	Cat# ab6326; RRID: AB_305426
Mouse monoclonal anti-Ddx6 (E12)	Santa Cruz	Cat# sc376433; RRID: AB_11151042
Rabbit polyclonal anti-Pax6	BioLegend	Cat# 901301; RRID: AB_2565003
Mouse monoclonal anti-Sox2 (E-4)	Santa Cruz	Cat# sc-365823; RRID: AB_10842165
Rat monoclonal anti-GFAP	Invitrogen	Cat# 13-0300; RRID: AB_2532994
Rabbit polyclonal anti-Sp8	Novus Biologicals	Cat# NBP249109
Rabbit polyclonal anti-Dlx5	Novus Biologicals	Cat# NBP185793; RRID: AB_11024022
Rabbit polyclonal anti-Arx	MyBioSource	Cat# MBS9606128
Rabbit monoclonal anti-Sox2	Cell Signaling	Cat# 3728; RRID: AB_2194037
Rabbit polyclonal anti-GFP	Abcam	Cat# ab13970; RRID: AB_300798
Mouse polyclonal anti-4E-T (IHC/IF)	Abcam	Cat# ab168098
Rabbit polyclonal anti-Cpeb4	Novus Biologicals	Cat# NBP181384; RRID: AB_11035231
Goat polyclonal anti-Ddx6	Invitrogen	Cat# PA5-18478
Rabbit polyclonal anti-4E-T (IP/Western)	Abcam	Cat# ab95030; RRID: AB_10675760
Rabbit polyclonal anti-Nestin	EMD Millipore	Cat# ab5922; RRID: AB_91107
Goat polyclonal anti-Pdgfra	R&D Systems	Cat# AF1062; RRID: AB_2236897
Mouse monoclonal anti-NeuN	EMD Millipore	Cat# MAB377; RRID: AB_2298772
Mouse monoclonal anti-HA.11	Covance/BioLegend	Cat# 901501; RRID: AB_2565006
Rabbit polyclonal anti-Cpeb4 (IF/IHC)	Novus Biologicals	Cat# NBP181384; RRID: AB_11035231
Rat monoclonal anti-Sox2	eBioscience	Cat# 14-9811-82; RRID: AB_11219471
Bacterial and virus strains		
NEB 5-alpha Competent E. coli (High Efficiency)	New England BioLabs	Cat# C2987H
Max Efficiency Stbl2 Competent Cells	Invitrogen	Cat# 10268-019
Chemicals, peptides, and recombinant proteins		
Cycloheximide (CHX)	Sigma Aldrich	Cat# C7698
5-Bromo-2′-deoxyuridine (BrdU)	Sigma Aldrich	Cat# B5002
Tamoxifen	Sigma Aldrich	Cat# T5648
4-OH-Tamoxifen	Sigma Aldrich	Cat# H7904
Critical commercial assays		
Magna RIP RNA-Binding Protein Immunoprecipitation Kit	EMD Millipore	Cat# 17-700
iScript cDNA Synthesis Kit	Bio-Rad	Cat# 1708890
SsoAdvanced Universal SYBR Green Supermix	Bio-Rad	Cat# 1725270
M.O.M (Mouse on Mouse) Immunodetection Kit	Vector	Cat# BMK-2202
Nextera XT DNA Library Preparation Kit	Illumina	CAT# FC-131-1024
Lipofectamine LTX Reagent with PLUS Reagent	Thermo Fisher Scientific	Cat# A12621
Direct-zol RNA Miniprep Plus Kit	Zymo Research	Cat# R2072

(*Continued on next page*)

Continued

REAGENT or RESOURCE	SOURCE	IDENTIFIER
Maxima H Minus First Strand cDNA Synthesis Master Mix, plus dsDNase	Thermo Fisher Scientific	Cat# M1681
Deposited data		
P6/P7 V-SVZ Single-cell RNA sequencing data	Borrett et al., 2020[86]	GEO: GSE152281
4E-T V-SVZ RIP-seq data	This paper	GEO: GSE224897 (Superseries GEO:GSE224857)
4E-T Neurosphere RIP-seq data	This paper	GEO: GSE224966
Cpeb4 V-SVZ RIP-seq data	This paper	GEO: GSE224896
P8 Neurosphere microarray data	This paper	GEO: GSE225351
RiboTag Neurosphere RIP-seq data	This paper	GEO: GSE224853
Cpeb4 Neurosphere RIP-seq data	This paper	GEO: GSE224854
Experimental models: Organisms/strains		
B6J.129(Cg)-Rpl22tm1.1Psam/SjJ	Jackson Laboratories	RRID: IMSR_JAX:029,977
C57BL/6-Tg(Nes-cre/ERT2)	Imayoshi et al., 2006[51]	https://doi.org/10.1002/dvg.20212
4E-T$^{fl/fl}$	Knockout Mouse Project (KOMP)	MGI:1921453; Eif4enif1$^{tm2a(KOMP)Wtsi}$
CD1 mouse strain	Charles River	Cat# 022, RRID: IMSR_CRL:022
Oligonucleotides		
shLuciferase: 5′-GGATTTCAGTCGATGTACA-3′	Yang et al., 2014[6]	N/A
sh4E-T: 5′-CCA TAG AGC TGA CTG GCT T-3′	Yang et al., 2014[6]	N/A
4E-T exon-specific primer, F: 5′-GGCCATCATGCCTCTCTGAA-3′	This paper	N/A
4E-T exon-specific primer, R: 5′-CCAGATCGTCGGGAGCTAAC-3′	This paper	N/A
For qPCR primers, please see Table S10	This paper	N/A
Recombinant DNA		
PiggyBac tGFP Plasmid	SBI Bioscience	Cat# PBSI506A-1
Super PiggyBac Transposase Plasmid	SBI Bioscience	Cat# PB210PA-1
Software and algorithms		
Volocity	Improvision	http://www.perkinelmer.com/lab-solutions/resources/docs/BRO_VolocityBrochure_PerkinElmer.pdf; RRID: SCR_002668
ZEN software	Zeiss Microscope	https://www.zeiss.com/microscopy/int/products/microscope-software/zen.html; RRID: SCR_013672
ImageJ	NIH	https://imagej.nih.gov/ij/docs/guide/user-guide.pdf; RRID:SCR_003070
GraphPad Prism	GraphPad	https://www.graphpad.com/scientific-software/prism/; RRID: SCR_002798
Adobe Illustrator	Adobe	http://www.adobe.com/products/illustrator.html; RRID: SCR_010279
Adobe Photoshop	Adobe	https://www.adobe.com/products/photoshop.html; RRID: SCR_014199
Affymetrix Expression Console Software	Thermo Fisher Scientific	http://www.affymetrix.com; RRID: SCR_010231
PANTHER Classification System (version 13.0)	Mi et al., 2013[84]	http://www.pantherdb.org/; RRID:SCR_004869
g:Profiler	Reimand et al., 2019[85]; Reimand et al., 2007[86]	http://biit.cs.ut.ee/gprofiler/gost; RRID:SCR_006809
Seurat R package	Laboratory of Rahul Satija	http://satijalab.org/seurat/; RRID:SCR_007322
DESeq2 version 1.26.0.	Bioconductor; Love et al., 2014[87]	https://bioconductor.org/packages/release/bioc/html/DESeq2.html; RRID:SCR_015687

RESOURCE AVAILABILITY

Lead contact

Further information and requests for resources and reagents should be directed to and will be fulfilled by the lead contact, Freda Miller (freda.miller@msl.ubc.ca).

Materials availability

Plasmids generated in this study and the *4et*$^{fl/fl}$ mice will be made available on request from the lead contact.

Data and code availability

- Previously published scRNA-seq datasets (from Borrett et al.[66]) are available under the ID code GEO: GSE152281. All of the new datasets presented here have been deposited in the GEO database under the ID code GEO: GSE224857 and are publicly available as of the date of publication. Specific accession numbers are listed in the key resources table.
- This paper does not report original code.
- Any additional information required to reanalyze the data reported in this paper is available from the lead contact upon request.

EXPERIMENTAL MODEL AND SUBJECT DETAILS

Mice

All animal use was approved by the Animal Care Committee of the Hospital for Sick Children in accordance with the Canadian Council on Animal Care policies. Mice were fed rodent chow and had free access to water in a 12-h dark-light cycle room. All mice were well maintained in a healthy state and no mouse displaying any signs of a health or behavioral abnormality was used in the study. For all studies, mice of either sex were used. The age of the mice used in the study ranged from embryonic day 15 (E15) to postnatal day 8 (P8). The specific ages of each animal for each experiment is documented in the results, method details and/or in the figure legends of the study. To obtain *4et*$^{fl/fl}$ mice, cryopreserved mutant C57BL/6 ES cells were purchased from the Knockout Mouse Project (Eif4enif1$^{tm2a(KOMP)Wtsi}$).[56,57] These harbored a *4et* allele containing a lacZ trapping cassette (knockout-first) and were used to generate chimeric mice which were subsequently crossed until the ES cells integrated into the germline. Mice heterozygous for the knockout-first *4et* allele were crossed to mice expressing flippase (FLP) recombinase[58] and this Flp-mediated recombination converted the knockout-first allele into a conditional allele containing *loxP* sites flanking critical exon 4 of *4et* (*4et*^{fl}). *4E-T*$^{fl/+}$ mice were backcrossed to wild type (*4et*$^{+/+}$) mice for several generations to remove the FLP recombinase, and finally crossed to one another to generate *4et*$^{fl/fl}$ homozygotes. To validate the generation of heterozygous (*4et*$^{fl/+}$), and homozygous (*4et*$^{fl/fl}$) knock-out first animals versus wild-types, PCR genotyping was used with the following primers:

CSD-F (AGCCCAGTATGGTGCTGCATGC); CSD-ttR (CAAATGAAACTGACAGTCCAGAACTCC); CAS_R1_Term (TCGTGGTAT CGTTATGCGCC). These primers produce a PCR product of 564bp for the *4et*^{fl} allele and 358bp for the *4et*$^{+}$ wt allele. Animals were crossed to *Nestin-CreERT2* (C57BL/6-Tg(Nes-cre/ERT2)[51] to generate the tamoxifen-inducible *4et*$^{fl/fl}$;*Nestin-CreERT2* mice. RiboTag transgenic mice (B6J.129(Cg)-Rpl22tm1.1Psam/SjJ)[80] were obtained from Jackson Laboratories. All transgenic mice were in a BL6 background and were bred and genotyped as recommended by Jackson Laboratories. Wild-type CD1 mice, used where indicated, were purchased from Charles River Laboratories.

METHOD DETAILS

BrdU and tamoxifen administration

For postnatal 4E-T ablation, *4et*$^{fl/fl}$*:Nestin-CreERT2* lactating female mice were injected 1 day post birth intraperitoneally with 1mg tamoxifen (Sigma Aldrich) in sunflower oil, twice daily for three days (P1-P3). To quantify proliferation, nursing female dams were injected with 100 mg/kg BrdU at P7 and the brains of littermate pups were dissected 24hrs later at P8 and prepared for immunostaining as described below.[67]

Cell cultures and transfections

The cerebral cortices of E15/16 embryos of either sex were dissected, the meninges were removed, and the excised neocortices were collected, pooled, and dissociated by mechanical trituration. The cell suspension was quantified and viability was determined by Trypan blue exclusion and cells were plated in Neurobasal medium (Invitrogen) supplemented with 1% penicillin/streptomycin (Lonza), 2% B27 (Invitrogen), 0.5mM L-glutamine (Invitrogen) and 40 ng/mL FGF (BD Biosciences) at a density of 200,000 cells/well on glass coverslips pre-treated with 2% laminin (BD Biosciences) and 1% poly-D-lysine (Sigma Aldrich) in 24-well plates.[81,82] Three hours post plating, wells were transfected with 0.5 μg PB tGFP vector expressing either *shLuciferase* or *sh4et* and 0.5 μg *Super PB* Transposase plasmids (PB210PA-1, SBI Biosciences) described below using Lipofectamine LTX (Fisher Scientific) per manufacturer's instructions.[81,83] Cells were cultured for 4.5 days as indicated, with medium changes in the interim.

Stable knockdown plasmid generation

shRNA targeting either Luciferase for control (5′-GGATTTCAGTCGATGTACA-3′) or 4E-T (5′-CCA TAG AGC TGA CTG GCT T-3′)[6] were cloned into a *PiggyBac* expression vector (PBSI506A-1, SBI Biosciences) encoding tGFP under control of the EF1α promoter and shRNA from the H1 promoter. Annealed forward and reverse oligos were inserted into the MCS of the PB expression vector via BamHI and EcoRI restriction sites and all resultant plasmids were validated by sequencing.[83] The Super PB transposase plasmid (PB210PA-1) was also purchased from SBI Bioscience and co-transfected as described above.[6,81,83]

Tissue preparation and immunostaining

Cells cultured on glass coverslips for the indicated times were fixed in 4% paraformaldehyde for 15 min at room temperature, permeabilized in 0.3% Triton-X100, then blocked for 1 h with 5% BSA. Coverslips were incubated in primary antibodies overnight at 4°C, washed in PBS, incubated in species-appropriate fluorophore-conjugated secondary antibodies for 1 h at room temperature, counterstained with Hoechst 33258 (Sigma Aldrich) and mounted onto glass slides with Permafluor (Fisher Scientific). For immunostaining the neonatal V-SVZ, the brains of postnatal pups at the indicated ages were dissected, fixed in 4% PFA at 4°C for 24 h, cryopreserved for 24–48 h in 30% sucrose, frozen at −80°C in OCT medium, and cryosectioned coronally at 16 μm. Sections were blocked and permeabilized for 1 h at room temperature in 0.3% Triton X-100 and 5% BSA and incubated with primary and secondary antibodies as above. For Ki67 tissue immunostaining, a mouse-on-mouse M.O.M kit (Vector Laboratories) was used as per manufacturer's instructions. To prepare adult brain sections for immunohistochemistry and FISH, P60 CD1 animals were perfused with RNAase-free 4% PFA, washed with PBS, fixed in 4% PFA for 24 h, submerged in 30% sucrose for an additional 48 h, then OCT-embedded and cyosectioned at 18 μm thickness. FISH and IHC were performed as described.

Antibodies

The antibodies used were as follows: mouse anti-Ki67 (BD Pharmingen, Cat# 550609, 1:200); mouse anti-Dlx2 (B-5) (Santa Cruz, Cat# sc-393879, 1:50); mouse anti-Olig2 (EMD Millipore, Cat# Mabn50, 1:500); rat anti-Ctip2 (Abcam, Cat# ab18465, 1:400); rabbit anti-BIII tubulin (BioLegend, Cat# 802001, 1:1000); rat anti-BrdU, (Abcam, Cat# ab6326, 1:200); mouse anti-Ddx6 (Santa Cruz, Cat# sc-376433, 1:100); mouse anti-Sox2 (E-4) (Santa Cruz, Cat# sc-365823, 1:200), rat anti-Sox2 (eBioscience, Cat# 14-9811-82, 1:1000); rat anti-GFAP (Invitrogen, Cat# 13-0300, 1:300), rabbit anti-Sp8 (Novus Biologicals, Cat# NBP249109, 1:100); rabbit anti-Dlx5 (Novus Biologicals, Cat# NBP185793, 1:500), rabbit anti-Arx (MyBiosource, Cat# MBS9606128, 1:200); rabbit anti-Sox2 (Cell Signaling, Cat# 3728; 1:500); chicken anti-GFP (Abcam, Cat# ab13970, 1:1000); mouse anti-4E-T (IF/IHC; Abcam; Cat# ab168098; 1:500); rabbit anti-Cpeb4 (IF/IHC; Novus Biologicals, Cat# NBP181384, 1:500); rabbit anti-Cpeb4 (IP/WB; Novus Biologicals, Cat# NBP1-80468, 10 μg); goat anti-Ddx6 (Invitrogen, Cat# PA5-18478, 1:100); rabbit anti-4E-T (IP/Western, Abcam, Cat# ab95030, 10 μg); rabbit anti-Nestin (EMD Millipore, Cat# ab5922, 1:1000); goat anti-PDGFRA (R&D Systems, Cat# AF1062, 1:100); mouse anti-NeuN (EMD Millipore, Cat# MAB377, 1:500); mouse anti-HA.11 (Covance/BioLegend, Cat# 901501, 1:100); anti-mouse and anti-rabbit IgG (EMD Millipore, Cat# 17-700, 10 μg). Fluorescently labeled highly cross-absorbed secondary antibodies were purchased from Invitrogen and used at a dilution of 1:1000.

Fluorescent *in situ* hybridization (FISH)

Cultured cells or cryosectioned slides were prepared as for immunostaining except with RNase-free conditions, were pre-incubated in hybridization buffer for 10 and 30 min respectively and the relevant probes from Molecular Instruments HCR RNA were added overnight at 37°C at a dilution of 0.4pmol/100μL as per manufacturer's instructions. Coverslips/slides were washed in wash buffer and sodium citrate with Triton X-100 solution, incubated in amplification buffer for 30 min at room temperature, then 6pmol of snap-cooled hairpin 1 and hairpin 2 diluted per 100 μL amplification buffer were added overnight at room temperature. Coverslips/sections were washed in sodium citrate buffer and either immunostained as described above or treated with Hoechst and mounting reagent. GFP probes were used as negative controls and positive signal was identified as punctate foci in the nucleus and cytoplasm.

Imaging, microscopy and quantifications

All images shown were taken on an Olympus IX81 spinning-disk confocal fluorescence microscope equipped with Hamamatsu C9100-13 EM-CCD camera and Yokogawa CSU X1 scanhead. Images were taken at 40-60× objective as Z-stacks with 0.3 μm optical slice thickness and processed with Volocity software (PerkinElmer). For quantification, images were captured using the Zeiss Axioplan2 with Axiocam (Zeiss) and X-Cite 120 LED lightsource and C11440 Hamamatsu camera, and analyzed using ZEN software (Zeiss) and ImageJ. To determine the number of marker-positive cells in the V-SVZ of postnatal coronal sections, at least 5 anatomically matched sections were quantified per brain from pups from at least three different litters, and results are presented as the total sum of cells positive per brain for the indicated marker. To analyze transfected cultures, 200–300 tGFP-positive cells were counted per experiment per condition for a minimum of three individual experiments defined as cultures derived from separate litters. Results are presented as the percent of cells double-positive for tGFP and the indicated marker relative to the total number of tGFP-positive cells counted. For analysis of "primed" cells in tissue sections, at least 5 sections were quantified per brain from at least three individual brains, where cells along the lateral V-SVZ expressing a minimum of 5 mRNA puncta and/or detectable protein were classified as positive for the marker. Results are presented as the percentage of cells expressing mRNA but not protein over the total number of mRNA-positive cells. To analyze transfected cultures, 200–300 tGFP-positive cells were counted per experiment per condition for a

minimum of three individual experiments defined as cultures derived from separate litters. Results are presented as the percent of cells double-positive for tGFP and the indicated marker relative to the total number of tGFP-positive cells counted.

Neurosphere cultures

Neurospheres were generated by dissecting the V-SVZ of the lateral ventricles of P7/8 CD1 or transgenic littermates as indicated, mechanically dissociated, and triturated into a single-cell suspension. Cell concentration and viability were determined by trypan blue exclusion and cells were then plated under clonal conditions at a density of 10 cells/uL in 6-well low-attachment dishes (Corning), with each brain cultured independently. Cells were maintained in DMEM and F12 medium supplemented with glucose, 2% B27 (Gibco), 10 ng/mL FGF (Corning), 20 ng/mL EGF (Corning), 2 μg/mL heparin (Stem Cell Technologies), 1% penicillin/streptomycin, and 0.5mM L-glutamine for 5 days, at which time 1 μM 4-hydroxy-tamoxifen (Sigma Aldrich) was added and spheres were cultured for a further 2–3 days as indicated. For quantification, 3 wells were counted and averaged per animal. To assay self-renewal and generate secondary spheres, primary neurospheres 2–3 days post Tamoxifen were dissociated mechanically by being sequentially passed through small-bore needles (McMaster Carr), filtered through a 70 μm strainer, counted, and replated in the same conditions as primary cultures, with each animal cultured individually. Secondary spheres were quantified in triplicates per animal at 7 days post plating.[67]

Western blotting

Cells were lysed in 1% NP-40 solution with 10% glycerol in TBST supplemented with Roche Protease and Phosphatase Inhibitors. Lysates were centrifuged at 13,000g for 10 min at 4°C, the supernatant was collected, and total protein concentration was quantified using the Pierce BCA Protein Assay Kit (Fisher Scientific); 5X Laemmli buffer with 1X DTT was added and samples were boiled for 5 min, run on MiniProtean TGX 4–20% gels (Bio-Rad), and transferred to 0.45 μm nitrocellulose membranes (Bio-Rad). Membranes were blocked for 1 h at room temperature in 5% BSA in PBS with 0.1% Tween-20, incubated with the appropriate primary antibodies overnight at 4°C, washed, and incubated with HRP-conjugated secondary antibodies of the corresponding species for 1 h at room temperature. Chemiluminescence reagents ECL Prime (Amersham) were used for detection.

Immunoprecipitation

Tissue from freshly-dissected P7/8 V-SVZs and cells from collected neurospheres were lysed on ice in Magna RIP Kit (EMD Millipore) lysis buffer supplemented with RNAse inhibitor and 1X Protease Inhibitor and protein content was quantified by Pierce BCA assay. 50 μL of Magna Protein A/G Magnetic beads were washed and bound to 10 μg of either IgG control of the appropriate species or the indicated antibody for 1.5 h at room temperature on a rotator. Cell lysates were equally divided between the IgG control and appropriate antibody-bead complexes, EDTA and RNAse inhibitor was added, and immunocomplexes were allowed to bind overnight at 4°C on a rotator. Immunocomplexes were washed 5–6 times using a magnetic separator and Laemmli buffer with SDS, DTT was added to immonocomplexes and samples were boiled for 5 min, extracted from the beads by magnetic separator, and run by western blot as described.

RNA immunoprecipitation sequencing (RIP-seq)

Tissue from freshly-dissected P7/8 V-SVZs and cells from collected neurospheres were lysed on ice in Magna RIP Kit (EMD Millipore) lysis buffer supplemented with RNAse inhibitor and 1X Protease Inhibitor and protein content was quantified by Pierce BCA assay. 50 μl of Magna Protein A/G Magnetic beads were washed and bound to 10 μg of either IgG control of the appropriate species or the indicated antibody for 1.5 h at room temperature on a rotator. Cell lysates were equally divided between the IgG control and appropriate antibody-bead complexes, EDTA and RNAse inhibitor was added, and immunocomplexes were allowed to bind overnight at 4°C on a rotator. Immunocomplexes were washed 5–6 times using a magnetic separator, protein was degraded and RNA was isolated using SDS and Proteinase K at 55°C for 30 min with agitation. RNA was extracted/purified with phenol-chloroform-isoamyl alcohol and chloroform, precipitated, washed, DNAse treated as per manufacturer's instructions (Magna RIP, EMD Millipore), and eluted in 10–15μl RNAse-free water.[7] Concentrations were measured by Qubit and RNA integrity was quantified by BioAnalyzer, cDNA was generated using the Takara Bio SMART-Seq v4 Low Input RNA Kit for Sequencing, and libraries were prepared using the Illumina Nextera XT DNA Library Preparation Kit. Libraries were sequenced on the Illumina HiSeq 2500 High Throughput flowcell paired-end 2x125bp or Novaseq SP flowcell paired-end 2x150bp with ~60 million reads per sample. Data quality was assessed by FastQC v.0.11.5, adaptors were trimmed using TrimGalore v.0.5.0, raw trimmed reads were aligned using STAR aligner, v.2.6.0c, and alignments were processed to obtain raw read counts for genes using htseq-count v.0.6.1p2. Two-condition differential gene expression analysis was performed with DESeq2[87] v.1.26.0. Where applicable, normalization/batch correction was performed by initial minimal filtering of 10 read counts per gene in at least 2 samples was applied to the datasets. More strict filtering to increase power is automatically applied via independent filtering on the mean of normalized counts within the DESeq results() function. All samples for each project were filtered and normalized together. Normalization is performed using the "median ratio method" (https://genomebiology.biomedcentral.com/articles/10.1186/gb-2010-11-10-r106), implemented by the estimateSizeFactors() function. The raw counts are divided by sample-specific size factors determined by median ratio of gene counts relative to geometric mean per gene. Differential expression testing was performed using the default Wald test. To control for batch effect the batch variable was added to the design formula. Further filters were applied and all non-protein coding genes were removed as well as genes

with an expression value of "0" counts in any sample or under "5" in the Cpeb4 or 4E-T samples. Transcripts were identified as 4E-T or Cpeb4-associated if the change of expression was at least 2-fold compared to the control IgG in the V-SVZ data and at least 1.75-fold in the neurospheres. Two independent experiments each were performed for Cpeb4 and 4E-T in the V-SVZ, two for 4E-T in neurospheres, and three for Cpeb4 in neurospheres. Gene ontology analysis for all enriched protein-coding genes over the indicated thresholds was performed by PANTHER (http://www.pantherdb.org/; RRID:SCR_004869;[84]) for protein class and g:Profiler for Biological Process, Molecular Function, and Human Phenotypes (http://biit.cs.ut.ee/gprofiler/gost; RRID:SCR_006809;[85,86]).

RiboTag analysis

NestinCreERT2$^{+/-}$ or wildtype animals were crossed to B6J.129(Cg)-Rpl22tm1.1Psam/SjJ homozygotes to generate the tamoxifen-inducible HA modification on Rpl22 (*Rpl22*$^{HA/HA}$) in Nestin-expressing precursors that are *CreERT2*-positive. Cells were derived from Cre^{+} P7/8 V-SVZ neurospheres where each animal was cultured independently and 1 μM 4-OH-tamoxifen (Sigma) was added after 5 days as described. Spheres were collected 2.5 days post-tamoxifen as indicated, triturated, counted by trypan blue exclusion, and were lysed in Magna RIP lysis buffer supplemented with 100 μg/mL of the translation inhibitor cycloheximide for stabilization of RNA–ribosome complexes, 1X protease and phosphatase inhibitor cocktail (Fisher Scientific), 200U/mL RNAsin (Promega) and heparin.[52–54] Lysates were centrifuged for 10 min at 4°C at 13,000g, and the supernatants of each condition (quantified using Pierce BCA kit) were divided and added to 50 μL of either Protein A/G magnetic bead-bound anti-HA antibody (Covance) or control Mouse IgG (EMD Millipore) at a concentration of 1:100 each and immunocomplexes were precipitated on a rotator overnight at 4°C. Complexes were washed 3–4 times in wash buffer supplemented with cycloheximide, RNAsin, and heparin as above, then washed twice in high salt buffer (MBL Bioscience). RNA extraction, sequencing, data analysis, and ontology analysis proceeded as described above for RIP-seq experiments. Further filters were applied removing all non-protein coding genes as well as genes with expression values of "0" in any sample or under "2" in HA samples for the three independent experiments performed. Ribosome-associated transcripts were identified as those at least 2-fold enriched in HA samples compared to IgG while ribosome-depleted were identified as those where the difference in HA versus IgG was <1, as described below. To ensure that only *NestinCre-ERT2*$^{+/-}$*; Rpl22*$^{HA/HA}$ (Cre+) cells incorporated the HA tag, and that Cre- cells did not, spheres were collected 2 days post-tamoxifen, run on westerns and immunoblotted with anti-HA antibody (Covance). To ensure the specificity of the anti-HA antibody, immunoprecipitation was performed with anti-HA and mouse IgG as above and lysates were analyzed on westerns that were probed with anti-HA.

Microarray analysis

Neurospheres prepared from the P8 V-SVZ as described above were lysed, RNA was extracted, and microarray analysis was performed for three replicates using MoGene-2.0st chips, as previously reported.[82]

Polysome fractionation and profiling

Primary neurospheres derived from the V-SVZ of CD1 P8 animals were cultured for 7 days as described, then treated with 100 μg/mL cycloheximide for 10 min at 37°C. Spheres were collected and triturated in cycloheximide-supplemented medium, counted, washed in PBS, pelleted, and snap-frozen. 15-30x10^{6} cells were used per experiment and fractionation was performed as reported using a sucrose gradient apparatus as described.[55] Briefly, cell pellets were lysed in buffer containing 20mM Tris-HCl, 100 mM KCl, 5mM MgCl2, 1% Triton-X 100, 0.5% sodium deoxycholate, 1mM DTT, and 100 μg/mL cycloheximide in RNAse-free water and on ice for 10 min. Tubes were centrifuged at 2,000g for 5 min, the supernatant was collected, centrifuged again at 13,000g for 5 min, and the resultant RNA concentration was measured using a UV-Vis spectrophotometer. Six 10–50% sucrose gradients were prepared using a 2.2M sucrose stock solution, salt solution, and cycloheximide in water and dispensed sequentially in ultracentrifuge tubes and left overnight at 4°C to establish the continuous/linear gradients. Sample lysates were subsequently loaded/overlaid on top of sucrose gradients in ultracentrifuge tubes and centrifuged at 190,000 x g at 4°C for 90 min, followed by fraction collection. Resultant sucrose fractions were pooled, with fractions 2–5 representing monosomes and 7–10 representing polysomes. 5 ng of *luciferase* mRNA spike-in control (Promega, Catalog No: L4561) was added to each condition. RNA was extracted using Direct-zol RNA Miniprep Plus kit (Zymo Research, Catalog No: R2072) and three volumes of Trizol LS (Thermo Fisher, Catalog No: 10296028) per manufacturer's instructions. A minimum of 1.5 μg RNA per condition was used to derive cDNA through reverse transcription with Maxima H Minus First Strand cDNA Synthesis Master Mix, plus dsDNase (Thermo Fisher, Catalog No: M1681), following manufacturer's protocol. RT-qPCR was conducted as described above and ΔΔCt method was employed to obtain fold changes using the *Luciferase* mRNA for normalization. Values for the indicated 4E-T target genes were derived by calculating Polysome:Monosome enrichment ratios and presenting the graph Y axis results as a percentage of the Polysome:Monosome ratio of positive control gene *Aldoc*.

Real-time quantitative PCR

Total RNA isolated using RNeasy (Qiagen) and extracted immunoprecipitated RNA were subjected to DNase treatment and reverse transcribed into cDNA using iScript Synthesis Kit (Bio-Rad) according to manufacturer's instructions. RT-qPCR was performed using Sso Advanced SYBR Green Supermix (Bio-Rad) with 1 μl of template on BioRad CFX96 Real-Time PCR Detection System. Data was quantified using the ΔΔCq method and CFX Maestro Software (Bio-Rad). Genes used for normalization/reference in RIP-RTqPCR

experiments were identified as unchanging between IgG and the specified antibody in the RIP-seqs and were as follows: *Tbp* for Ribotag experiments, *Tubb2a* and *Tubb5* for 4E-T V-SVZ immunoprecipitates, *Ywhag* and *Rpl8* for Cpeb4 V-SVZ immunoprecipitates, *Rpl28* for 4E-T neurosphere immunoprecipitates, and *Ube4a* for Cpeb4 neurosphere immunoprecipitates. Please see Table S10 for a complete list of qPCR primer sequences. For 4E-T knockout validation, total RNA was extracted from primary neurospheres derived from tamoxifen-treated *Nestin-CreERT2*$^{+/-}$;*4et*$^{fl/fl}$ (Cre^{+}) and *4et*$^{fl/fl}$ (Cre-) animals cultured individually as described and the reaction was prepared by DreamTaq Hot Start PCR Master Mix (Fisher Scientific) using primers designed to span floxed Exon 4. The Forward primer (5′-GGCCATCATGCCTCTCTGAA-3′) was generated against Exon 3 and the Reverse primer (5′-CCAGAT CGTCGGGAGCTAAC-3′) was generated against Exon 5, producing a PCR product of 270bp for Cre- and 143bp for Cre+ when run by electrophoresis in 2% agarose gel. *Rpl8* was used as control/reference gene.

scRNA-seq analysis

Previously-published scRNA-seq data (Borrett et al.[66]; GEO accession GSE152281) were analyzed using approaches described in detail in Borrett et al.[66] Violin plots for dNSC, TAP, and Neuroblast clusters were generated using the Seurat VlnPlot function, and heatmaps were generated using the Seurat DoHeatmap function using scaled expression values where violet indicates lower expression and yellow indicates higher expression.

QUANTIFICATION AND STATISTICAL ANALYSIS

Quantification of RiboTag experiments

Three independent neurosphere RiboTag experiments were performed as described. For each experiment for each protein-coding mRNA, the fold-change in the HA-tagged immunoprecipitate versus the control IgG immunoprecipitate was determined, and total, 4E-T target or Cpeb4 target mRNAs were binned by expression level as a percentage of total mRNAs in that dataset. In addition to analyzing each experiment independently, the three experiments were analyzed as a group, calculating the group log2 fold change taking all replicates and the variability between them into consideration using DESeq2[87] as described above. This grouped fold change (Table S7) was used to compile the list of 4E-T ribosome-associated and ribosome-depleted target mRNAs for the gene ontology in Figures 5H and 5I and in Table S9.

Quantification of marker-positive cells in 4E-T ablation *in vivo* experiments

Coronal sections encompassing the V-SVZ from P8 tamoxifen-treated *4et*$^{fl/fl}$; *Nestin-CreERT2* brains were immunostained with the indicated antibodies as described. For quantification, images were captured using the Zeiss Axioplan2 with Axiocam (Zeiss) and X-Cite 120 LED lightsource and C11440 Hamamatsu camera, and analyzed using ZEN software (Zeiss) and ImageJ. To determine the number of marker-positive cells in the V-SVZ, at least 5 anatomically matched V-SVZ sections were quantified per brain from pups from at least three different litters, and results are presented as the total sum of cells positive in the same number of sections per brain for the indicated marker. In all scatter plots each data point/replicate represents an individual brain.

Quantification of marker-positive cells in 4E-T knockdown *in vitro* experiments

To analyze cultures transfected and immunostained as described, at least 3 cover slips per experiment per condition were counted for a total of 200–300 tGFP-positive cells per condition. Individual experiments are defined as cultures derived from separate litters, and at least 3 independent experiments were performed per condition. Results are presented as the percent of cells double-positive for tGFP and the indicated marker relative to the total number of tGFP-positive cells counted. For quantification, images were captured using the Zeiss Axioplan2 with Axiocam (Zeiss) and X-Cite 120 LED lightsource and C11440 Hamamatsu camera, and analyzed using ZEN software (Zeiss) and Image J.

Quantification of marker-positive cells in the perinatal and adult V-SVZ

For Dlx2, coronal sections of P5 and P60 CD1 brains were analyzed by FISH and immunostaining, as described. Images were obtained on an Olympus IX81 spinning-disk confocal fluorescence microscope equipped with Hamamatsu C9100-13 EM-CCD camera and Yokogawa CSU X1 scanhead. Images were taken at 40-60X objective as Z-stacks with 0.3 μm optical slice thickness and processed with Volocity software (PerkinElmer). At least 5 sections were quantified per brain from at least three individual brains, where cells along the lateral V-SVZ expressing a minimum of 5 mRNA puncta and/or detectable protein were classified as positive for the marker. Results are presented as the percentage of cells expressing mRNA but not protein over the total number of mRNA-positive cells. To quantify 4E-T or Cpeb4-positive Sox2-expressing cells, coronal sections of P5 and P60 CD1 brains were immunostained as described and images obtained as for Dlx2. Images were quantified using ImageJ software, and at least 5 V-SVZ sections per brain for three brains of each time point were quantified for total Sox2-positive cells as well as Sox2-positive cells expressing punctate 4E-T or Cpeb4. Results are represented as the percent of Sox2-positive V-SVZ cells expressing the punctate marker over total Sox2-positive cells.

Statistical analysis

All graphs are presented as mean with standard deviation (SD). For all analyses between two groups/conditions, statistical significance was assessed by the two-tailed unpaired Student's t-test where the significance threshold was $p < 0.05$. For comparisons entailing multiple groups (Figures 5D, 5E, and 5G), one-way ANOVA was used followed by Dunnett's multiple comparisons post hoc test analyzing the mean of each column compared to the mean of the ribosome-associated column (HA/IgG >2). Graphpad Prism 9.3.1 was used for all comparisons. As indicated in figure legends, asterisks denote statistical significance and error bars the standard deviation.